REPORT DOCUMENTATION PAGE

Form Approved OMB NO. 0704-0188

1. REPORT DATE (DD-MM-YYYY)	2. REPORT TYPE	3. DATES COVERED (From - To)
23-04-2015	Final Report	-

4. TITLE AND SUBTITLE

Understanding and Migitating Vortex-Dominated, Tip-Leakage and End-Wall Losses in a Transonic Splittered Rotor Stage - Final Report

5a. CONTRACT NUMBER

5b. GRANT NUMBER

ARO MI-PR--

5c. PROGRAM ELEMENT NUMBER

611102

6. AUTHORS

Garth Hobson, Anthony Gannon

5d. PROJECT NUMBER

5e. TASK NUMBER

5f. WORK UNIT NUMBER

7. PERFORMING ORGANIZATION NAMES AND ADDRESSES

Naval Postgraduate School (NPS-Monterey) 14,973.00
1 University Circle

Monterey, CA 93943 -5000

8. PERFORMING ORGANIZATION REPORT NUMBER

9. SPONSORING/MONITORING AGENCY NAME(S) AND ADDRESS (ES)

U.S. Army Research Office
P.O. Box 12211
Research Triangle Park, NC 27709-2211

10. SPONSOR/MONITOR'S ACRONYM(S)
ARO

11. SPONSOR/MONITOR'S REPORT NUMBER(S)

60039-EG.6

12. DISTRIBUTION AVAILIBILITY STATEMENT

Approved for public release; distribution is unlimited.

13. SUPPLEMENTARY NOTES

The views, opinions and/or findings contained in this report are those of the author(s) and should not contrued as an official Department of the Army position, policy or decision, unless so designated by other documentation.

14. ABSTRACT

The requirement for higher power-to-weight ratios in modern jet engines leads to a reduced number of stages at increased loading per stage or blade row. Splittered, blade rows enable a large flow deflection and a correspondingly high-pressure rise within a short distance. In the 1970's Wennerstrom and Hearsey [1] undertook the task of designing, building and testing a supersonic axial flow stage with a pressure ratio of 3.0 and an isentropic efficiency of 0.82. Upon testing, the stage fell dramatically short of design. This was blamed largely on poor flow control within the rotor passage. Recognizing the splitters had long been used to improve performance of

15. SUBJECT TERMS

Tip Leakage, Vortex, Axial Compressor

16. SECURITY CLASSIFICATION OF:			17. LIMITATION OF ABSTRACT	15. NUMBER OF PAGES	19a. NAME OF RESPONSIBLE PERSON
a. REPORT	b. ABSTRACT	c. THIS PAGE			Garth Hobson
UU	UU	UU	UU		19b. TELEPHONE NUMBER: 831-656-2888

Report Title

Understanding and Migitating Vortex-Dominated, Tip-Leakage and End-Wall Losses in a Transonic Splittered Rotor Stage - Final Report

ABSTRACT

The requirement for higher power-to-weight ratios in modern jet engines leads to a reduced number of stages at increased loading per stage or blade row. Splittered, blade rows enable a large flow deflection and a correspondingly high-pressure rise within a short distance. In the 1970's Wennerstrom and Hearsey [1] undertook the task of designing, building and testing a supersonic axial flow stage with a pressure ratio of 3.0 and an isentropic efficiency of 0.82. Upon testing, the stage fell dramatically short of design. This was blamed largely on poor flow control within the rotor passage. Recognizing the splitters had long been used to improve performance of centrifugal compressors, the decision was made to use a splitter, in the hopes that better flow control could be achieved without incurring additional losses [2]. Due to time constraints, many decisions regarding the splitter were based upon engineering judgment with little analysis. The result of adding the splitter was that the rotor performance improved, but the overall stage performance was still short of the goal, as the pressure ratio was 2.76 and the efficiency was only 0.68. However the stage was much less sensitive to incidence variations at off-design conditions, indicating that the splitter did indeed improve the flow control within the rotor [3].

Inviscid and viscous, three-dimensional calculations were performed by Tzuoo, et. al. [4] in 1990 on Wennerstrom's rotor. They determined that additional shocks existed between the splitter vanes and main airfoils and they also noted that by moving the splitter closer to the main airfoil suction side the likelihood of passage choking was reduced. Most recently, McGlumphy, et. al. [5] performed a numerical study on a rear stage of a core compressor that incorporated splitter vanes on the rotor. The shock-free fully turbulent flow analysis showed that the tandem rotor outperformed its single blade counterpart by attaining a higher, pressure ratio and efficiency as well as numerical stall margin. In spite of all these advancements splittered or tandem rotors have not been used on rotors and hence the lack of use is the motivation for the current study.

Both the location of the splittered blade as well as the tip section profile, of both the main blade and splittered blade, can be optimized to mitigate tip leakage and end wall flows. Since computational analysis has matured to the level where design optimization can be performed with such variables as airfoil shape and spacing of the main and splitter blades. As clearance-to-span ratios increase in high-pressure ratio compressors, so too will the chord-to-clearance ratio. Hence the logical conclusion to attempt to overcome the associated tip clearance loss with strategically placed partial blades within the main passage.

Enter List of papers submitted or published that acknowledge ARO support from the start of the project to the date of this printing. List the papers, including journal references, in the following categories:

(a) Papers published in peer-reviewed journals (N/A for none)

Received	Paper

TOTAL:

Number of Papers published in peer-reviewed journals: 0.00

(b) Papers published in non-peer-reviewed journals (N/A for none)

Received	Paper

TOTAL:

Number of Papers published in non peer-reviewed journals: 0.00

(c) Presentations

Number of Presentations: 0.00

Non Peer-Reviewed Conference Proceeding publications (other than abstracts):

Received	Paper

TOTAL:

Number of Non Peer-Reviewed Conference Proceeding publications (other than abstracts): 0

Peer-Reviewed Conference Proceeding publications (other than abstracts):

Received	Paper	
01/17/2015	3.00	Garth Hobson, PhD, Anthony Gannon, PhD, Scott Drayton, LCDR USN. DESIGN AND TEST OF A TRANSONIC AXIAL SPLITTERED ROTOR, ASME TURBO Expo 2015. 15-JUN-15, . : ,
01/22/2015	4.00	Anthony J. Gannon , Garth V. Hobson, Mark G. Turner, Wolfgang Sanz. PERFORMANCE OF A SPLITTERED TRANSONIC ROTOR WITH SEVERAL TIP CLEARANCES, ASME Turbo Expo 2015. 15-JUN-15, . : ,
01/22/2015	5.00	Mark G. Turner, Ahmed Nemnem, Anthony Gannon, Garth Hobson, Wolfgang Sanz. MEASURED HEAT TRANSFER IN A TRANSONIC FAN RIG AT CASING WITHIMPLICATIONS ON PERFORMANCE, ASME Turbo Expo 2015. 15-JUN-15, . : ,
TOTAL:	**3**	

Number of Peer-Reviewed Conference Proceeding publications (other than abstracts): 0

(d) Manuscripts

Received	Paper
TOTAL:	

Number of Manuscripts: 0.00

Books

Received	Book
TOTAL:	

Received	Book Chapter

TOTAL:

Patents Submitted

Patents Awarded

Awards

Graduate Students

NAME	PERCENT_SUPPORTED

FTE Equivalent:
Total Number:

Names of Post Doctorates

NAME	PERCENT_SUPPORTED

FTE Equivalent:
Total Number:

Names of Faculty Supported

NAME	PERCENT_SUPPORTED

FTE Equivalent:
Total Number:

Names of Under Graduate students supported

NAME	PERCENT_SUPPORTED

FTE Equivalent:
Total Number:

Student Metrics

This section only applies to graduating undergraduates supported by this agreement in this reporting period

The number of undergraduates funded by this agreement who graduated during this period: 0.00

The number of undergraduates funded by this agreement who graduated during this period with a degree in science, mathematics, engineering, or technology fields:..... 0.00

The number of undergraduates funded by your agreement who graduated during this period and will continue to pursue a graduate or Ph.D. degree in science, mathematics, engineering, or technology fields:..... 0.00

Number of graduating undergraduates who achieved a 3.5 GPA to 4.0 (4.0 max scale):..... 0.00

Number of graduating undergraduates funded by a DoD funded Center of Excellence grant for Education, Research and Engineering:..... 0.00

The number of undergraduates funded by your agreement who graduated during this period and intend to work for the Department of Defense 0.00

The number of undergraduates funded by your agreement who graduated during this period and will receive scholarships or fellowships for further studies in science, mathematics, engineering or technology fields: 0.00

Names of Personnel receiving masters degrees

NAME

Total Number:

Names of personnel receiving PHDs

NAME

Total Number:

Names of other research staff

NAME PERCENT_SUPPORTED

FTE Equivalent:
Total Number:

Sub Contractors (DD882)

Inventions (DD882)

Scientific Progress

Technology Transfer

UNDERSTANDING AND MITIGATING VORTEX-DOMINATED, TIP-LEAKAGE AND END-WALL LOSSES IN A TRANSONIC SPLITTERED ROTOR STAGE.

Garth V. Hobson and Anthony J. Gannon
Turbopropulsion Laboratory
Naval Postgraduate School
Department of Mechanical and Aerospace Engineering
700 Dyer Rd, Monterey
CA 93940, USA

ABSTRACT

The requirement for higher power-to-weight ratios in modern jet engines leads to a reduced number of stages at increased loading per stage or blade row. Splittered, blade rows enable a large flow deflection and a correspondingly high-pressure rise within a short distance. In the 1970's Wennerstrom and Hearsey [1] undertook the task of designing, building and testing a supersonic axial flow stage with a pressure ratio of 3.0 and an isentropic efficiency of 0.82. Upon testing, the stage fell dramatically short of design. This was blamed largely on poor flow control within the rotor passage. Recognizing the splitters had long been used to improve performance of centrifugal compressors, the decision was made to use a splitter, in the hopes that better flow control could be achieved without incurring additional losses [2]. Due to time constraints, many decisions regarding the splitter were based upon engineering judgment with little analysis. The result of adding the splitter was that the rotor performance improved, but the overall stage performance was still short of the goal, as the pressure ratio was 2.76 and the efficiency was only 0.68. However the stage was much less sensitive to incidence variations at off-design conditions, indicating that the splitter did indeed improve the flow control within the rotor [3].

Inviscid and viscous, three-dimensional calculations were performed by Tzuoo, et. al. [4] in 1990 on Wennerstrom's rotor. They determined that additional shocks existed between the splitter vanes and main airfoils and they also noted that by moving the splitter closer to the main airfoil suction side the likelihood of passage choking was reduced. Most recently, McGlumphy, et. al. [5] performed a numerical study on a rear stage of a core compressor that incorporated splitter vanes on the rotor. The shock-free fully turbulent flow analysis showed that the tandem rotor outperformed its single blade counterpart by attaining a higher, pressure ratio and efficiency as well as numerical stall margin. In spite of all these advancements splittered or tandem rotors have not been used on rotors and hence the lack of use is the motivation for the current study.

Both the location of the splittered blade as well as the tip section profile, of both the main blade and splittered blade, can be optimized to mitigate tip leakage and end wall flows. Since computational analysis has matured to the level where design optimization can be performed with such variables as airfoil shape and spacing of the main and splitter blades. As clearance-to-span ratios increase in high-pressure ratio compressors, so too will the chord-to-clearance ratio. Hence the logical conclusion to attempt to overcome the associated tip clearance loss with strategically placed partial blades within the main passage.

OBJECTIVES

The main objective of this project is to maximize the performance of a single transonic compressor stage by reducing the number of blades that produce shockwaves off their leading edges with half the associated tip leakage flow in the casing region. If half the number of blades can be used to reduce the flow to subsonic speeds then additional, splitter, blades can be used to turn the flow with realistic diffusion factors in the aft subsonic region as shown schematically in Fig 1. The tip leakage flow for this "staged" compression on a single impeller should be less severe than fully bladed rotors. The added benefit of the splitter blade operating in the "wake" of the tip leakage vortex of the main blade (Fig. 2a) as described by Smith [6]. The lower solidity of the main "transonic" airfoils should mitigate spillage of the tip leakage flow around the adjacent leading edge when operating close to stall (Fig. 2b). The splitter blade will also be able to alter the flow of the tip clearance backflow at the trailing edge as computed by Vo [7]. Both these effects should be able to control any potential "spike-type" compressor stall inception as described by Tan et al [8]. Splittered rotors have been used successfully for decades in centrifugal compressors where the clearance-to-span ratios are much higher than axial compressors. Additionally splittered centrifugal compressors produce higher pressure ratios than fully bladed rotors and hence these could have the same benefit in axial compressors.

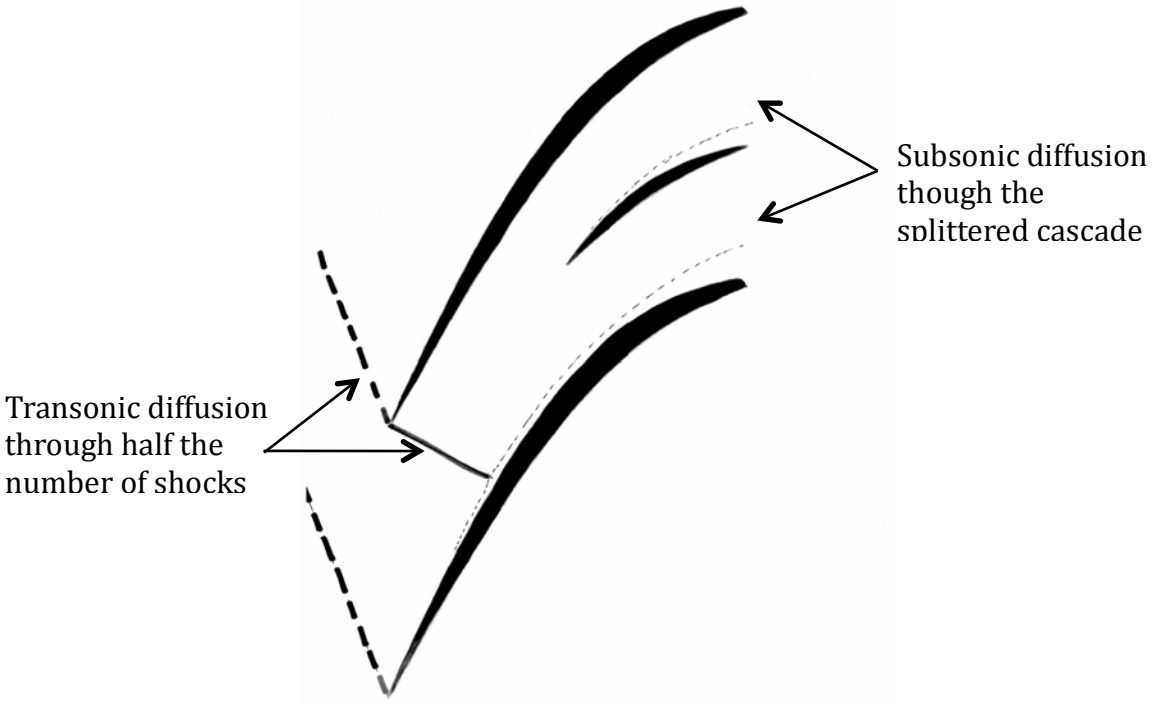

Fig. 1, Schematic of the Wennerstrom and Hearsey [1] Splittered Rotor Concept.

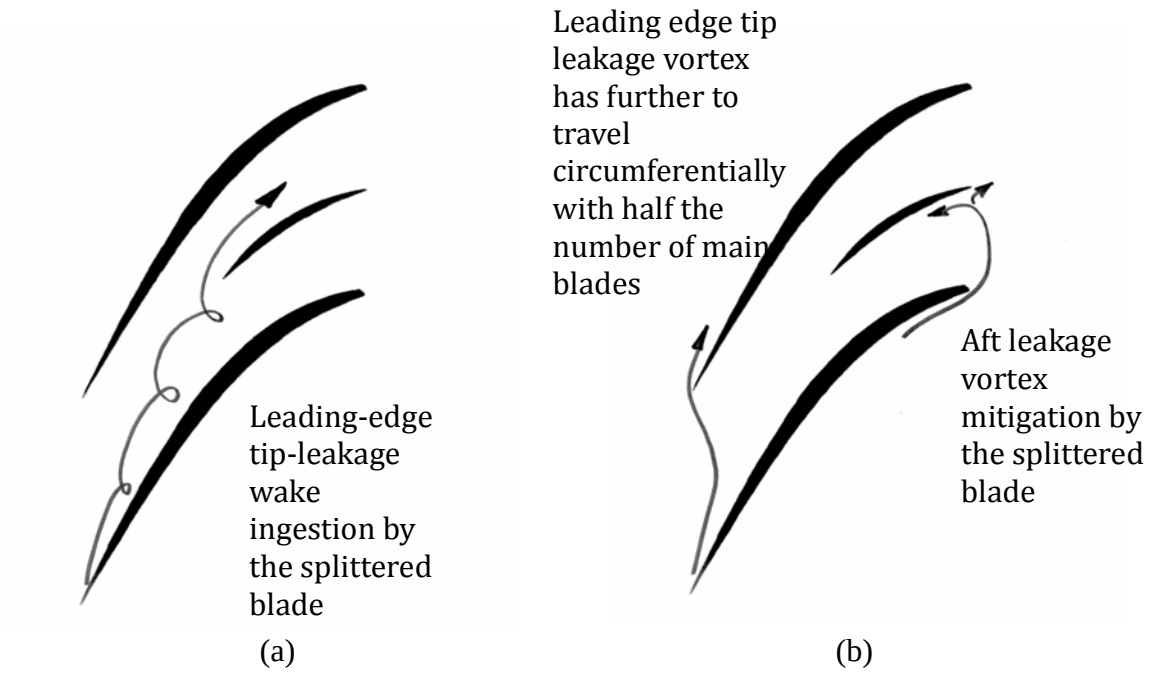

Fig. 2, Splittered rotor tip leakage flows at; (a) peak efficiency and (b) near stall.

Bhargava & Gopalakrishnan [9], Ogawa & Gopalakrishnan [10 & 11], and Fabri [12] performed computations on splittered centrifugal compressors in low speed flows. Millour [13] examined the same configuration using a 3D Euler analysis with simplified viscous forces. All noted that the primary effect of the splitters (aft blades) is to decrease the loading on the main blades, as well as to reduce the jet/wake effect at the rotor exit. McGlumphy [14] computed the flow through an overlapped tandem, or partial splittered rotor, for purely axial flow. He observed that in the tip region the aft blade losses decreased so much that they were below the 2-D cascade value. When considering the predicted streamline visualization of the tip leakage flow as shown in Fig. 3, a major portion of the tip vortex migrated across the passage into the aft blade clearance region. He speculated that the injection of additional fluid through the aft blade tip gap helped reduce the losses there and further redistributed the radial flow.

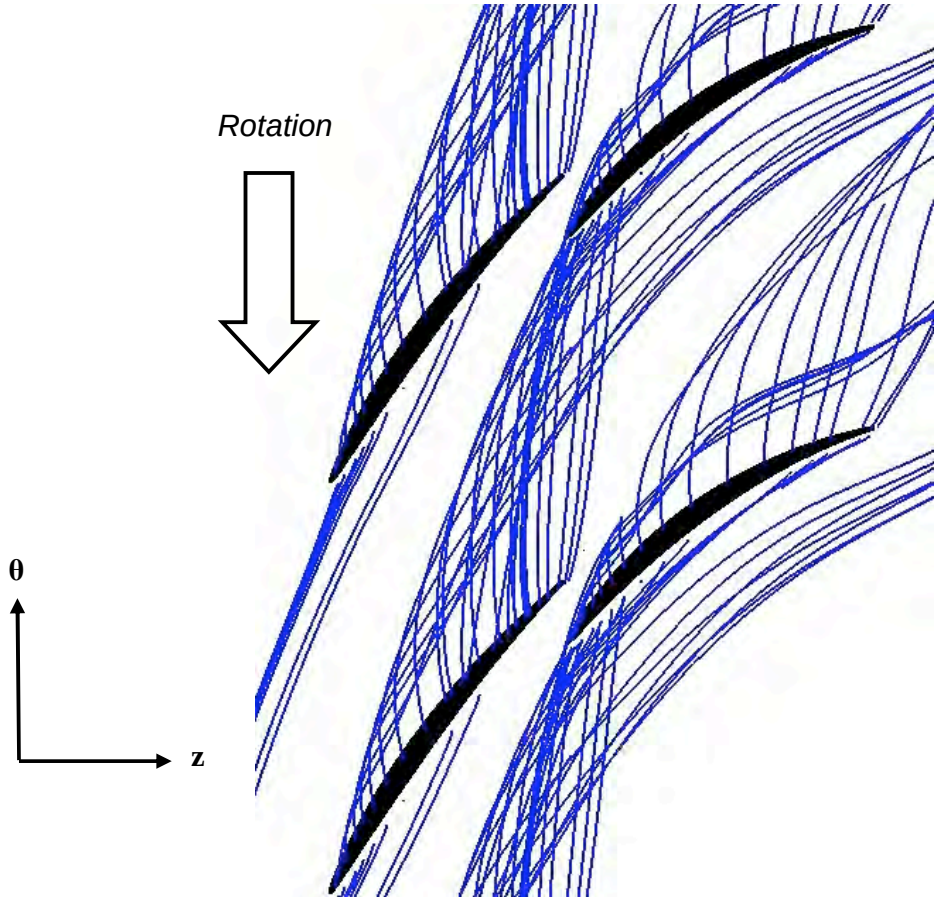

Fig. 3, Top View of Tip Clearance Streamlines (Reproduced by permission) [McGlumphy, 14]

TECHNICAL APPROACH AND METHODOLOGY

Adaptation of Sanger Preliminary Design Method

In the 1990s, a transonic axial rotor–stator stage was designed by Nelson L. Sanger of NASA Lewis Research Center exclusively for the Naval Postgraduate School as a research and teaching tool. Sanger's transonic axial compressor rotor is shown in Fig 4. The design process and methodology followed is documented in Sanger [15, 16], which resulted in a low aspect ratio (1.2) rotor with a tip relative inlet Mach number of 1.3, and an overall stage pressure ratio of 1.57. Over the course of approximately ten years experimental and numerical investigations evaluated the Sanger compressor performance over a variety of operating speeds and conditions.

Fig. 4, Sanger's transonic axial compressor rotor [17].

Having proven that the Sanger design methodology was robust by extensive performance evaluation, parts of his work were adapted as a starting point for the design portion of this study. The preliminary design steps, which he followed and documented in detail [16], were coded in a MATLAB script. Initially the Sanger method required ambient conditions, gas properties and the input design parameters such as stagnation pressure ratio (PR), efficiency (h), aspect ratio (AR), stagger angle (SA), specific weight flow (W), axial velocity ratio (AVR), inlet and exit tip radii and the exit hub radius (TIR, TER and HER).

To provide a more accurate estimate of the blade angles required to start the design process for the transonic conditions of the splitter rotor passage, a normal shock was assumed to be situated in the passage as shown in Fig 5.

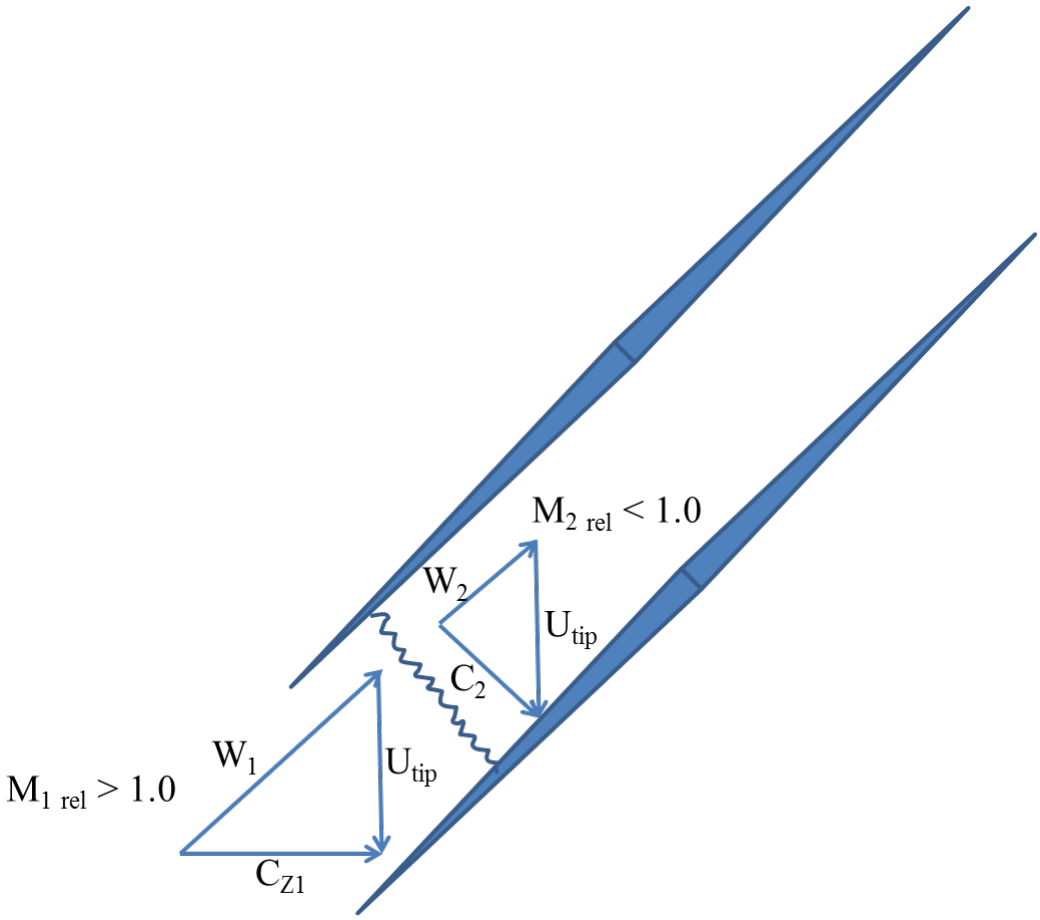

Fig. 5, Loss model based on a single normal shock in passage.

Calculations to construct the inlet velocity triangle were completed using the blade tip Mach number calculated earlier using the Sanger method. Starting with the inlet relative Mach number at the tip as well as the specified AVR, a normal shock wave was computed using equation (1) to determine the downstream relative subsonic Mach number and associated velocity (W_2) shown in Fig 6.

$$M^2_{2rel} = \frac{M^2_{1rel} + \frac{2}{\gamma - 1}}{\left(\frac{2\gamma}{\gamma - 1}\right)\left(M^2_{1rel} - 1\right)} \qquad (1)$$

The inlet and outlet velocity triangles are combined to show the net turning resulting from a normal shock located in the rotor passage. The combined velocity triangle with an AVR of 0.90 is shown in Fig 6, after subsonic turning of the flow aft of the shock.

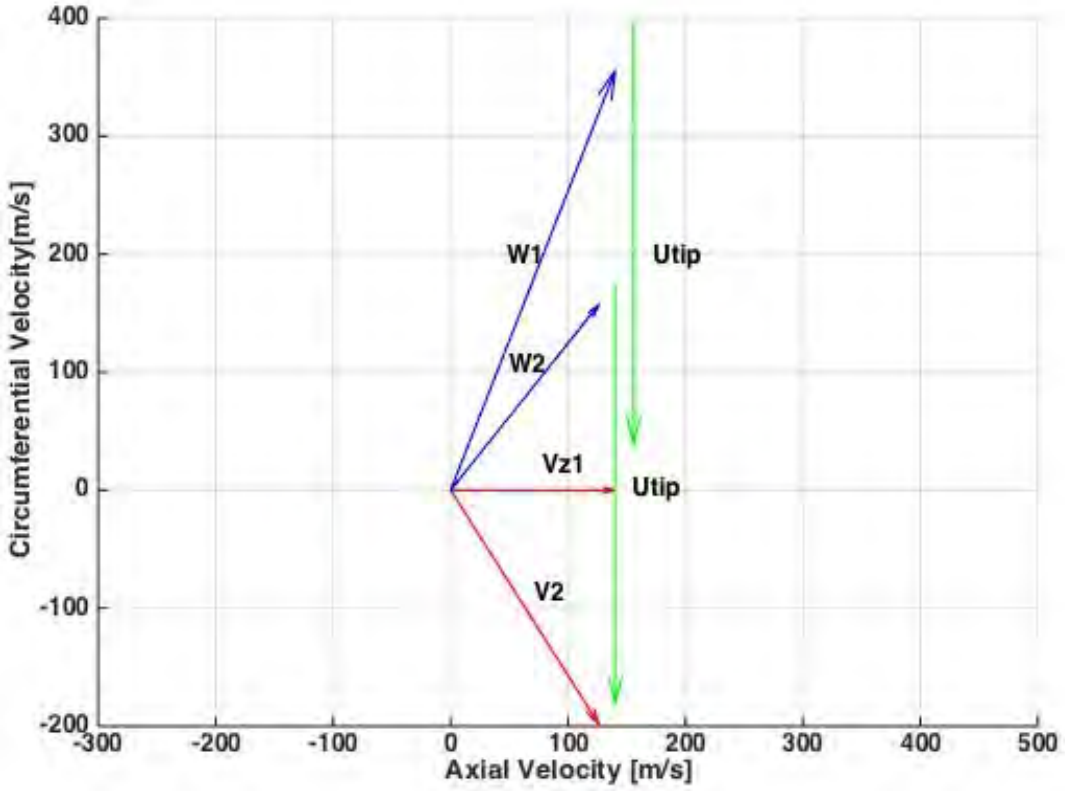

Fig. 6, Rotor tip section combined velocity triangles.

Automation

Recent computational fluid dynamics (CFD) studies at the Turbopropulsion Laboratory (TPL) have made extensive use of SolidWorks, a commercial solid modeling program, and ANSYS Workbench, a commercial simulation package that includes amongst others mesh generation, structural analysis, modal analysis, and CFD modules. The gas path analysis methods used in those previous studies are well documented in Boyter [18] and McNab [19]. Rotor gas path solid models were developed in SolidWorks and then imported into ANSYS CFX for performance analysis. The interface between SolidWorks and ANSYS required manual intervention. Any changes to the rotor gas path solid model required human-in-the-loop modification followed by manual updating of ANSYS Design Modeler and refreshing of ANSYS CFX setup for performance analysis. Additionally, to predict the data required to produce a rotor performance map, throttling needed to occur via manual manipulation of the rotor gas path outlet pressure.

Given this study's objectives and time constraints, it was apparent a design tool that automated geometry generation and CFD analysis as well as the interface between the standalone commercial software packages SolidWorks and ANSYS was required. MathWorks' MATLAB technical computing language was chosen as the software package to interface with SolidWorks and ANSYS Workbench. Versions MATLAB R2012b, SolidWorks 2010, and ANSYS

Workbench 14.0 were used in this study. The resultant design tool process flow chart is shown in Fig 7.

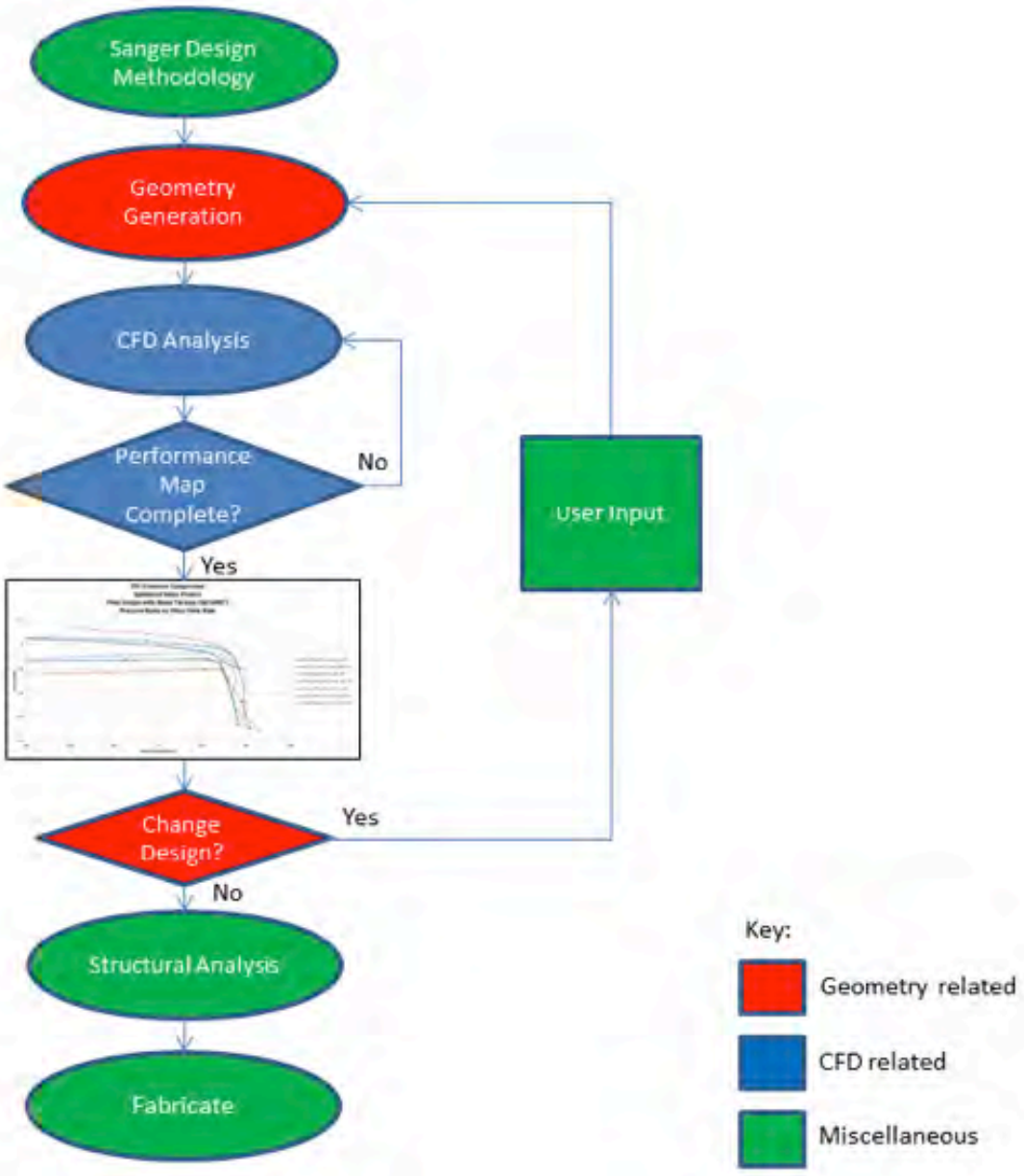

Fig. 7, Design process flow chart.

To begin the design process, the Sanger design methodology with the incorporated shock loss model was used to produce inlet and outlet velocity triangles. From these velocity triangles, overall stage flow turning angles were calculated and used to guide the user inputs for blade angles and thickness distributions. Armed with basic blade geometry parameters the TPL design

tool was initiated by running the MATLAB script (*.m) Main_SpeedLine_Auto. Main_SpeedLine_Auto called the following MATLAB scripts:

- HardCodeBlade
- HardCodeParams

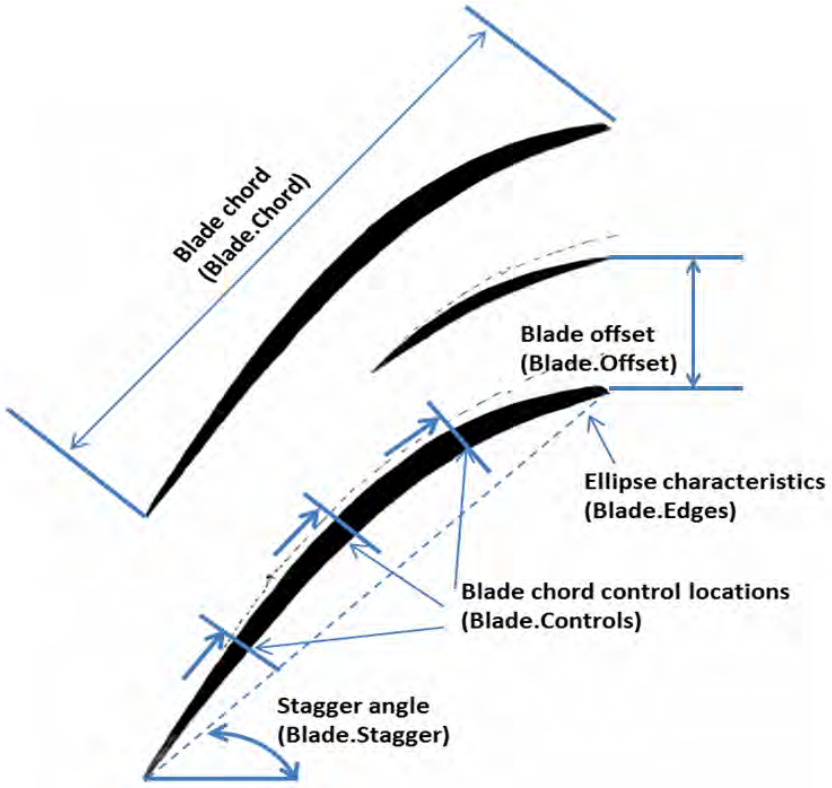

Fig. 8, HardCodeBlade blade input parameters.

Some of the blade input parameters and passage input parameters are shown in Figs 8 and Fig 9 respectively.

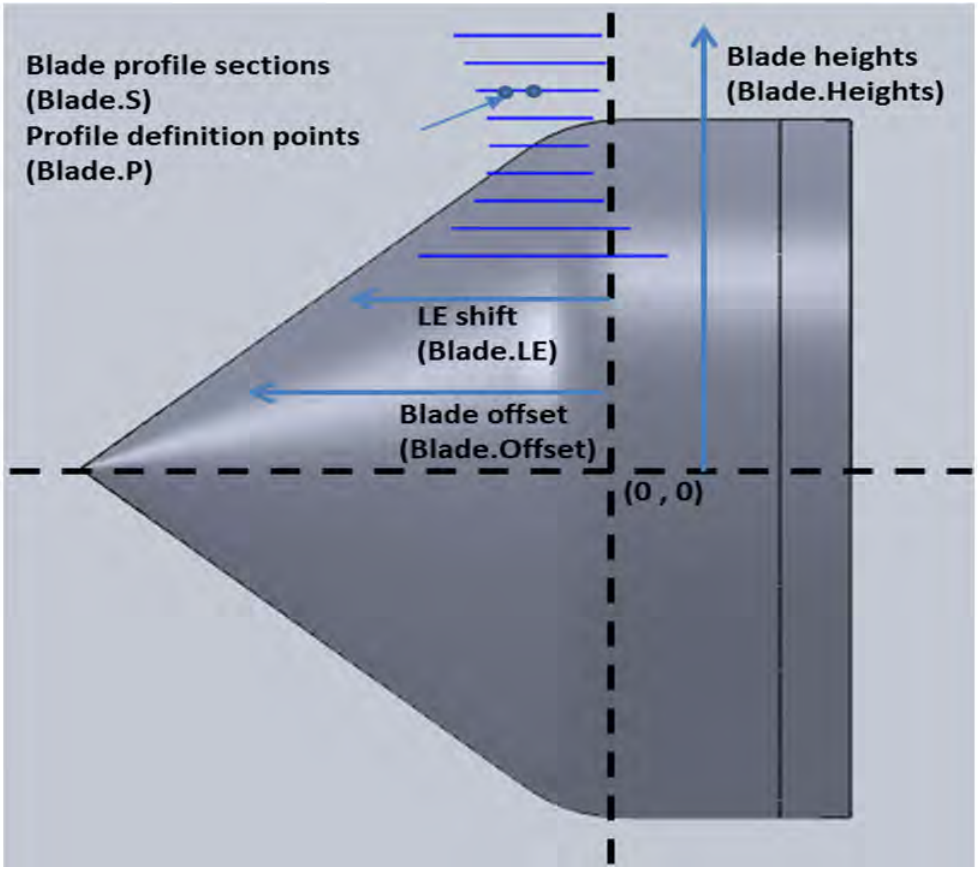

Fig. 9, HardCodeBlade passage input parameters.

The GeomGen script was the main routine responsible for blade, hub, spinner, and casing geometry generation and rotor and air wedge solid model generation in SolidWorks. To accomplish this GeomGen called the following seven MATLAB scripts:

- BladeGen
- SangerMethod
- Passage
- WedgeGen
- StreamGen
- SolidWorksGen
- BladeHub_Wedge_CutOut

Using the parameters passed in and described above, bladegen started the blade profile generation process by calling the bladesect script. Depending on the number of blade sections prescribed earlier, bladegen generated blade sections by repeatedly calling bladesect for both the main blade and splitter blade. Bladesect used a third-order spline between control points for camber line distribution as shown in Fig 10.

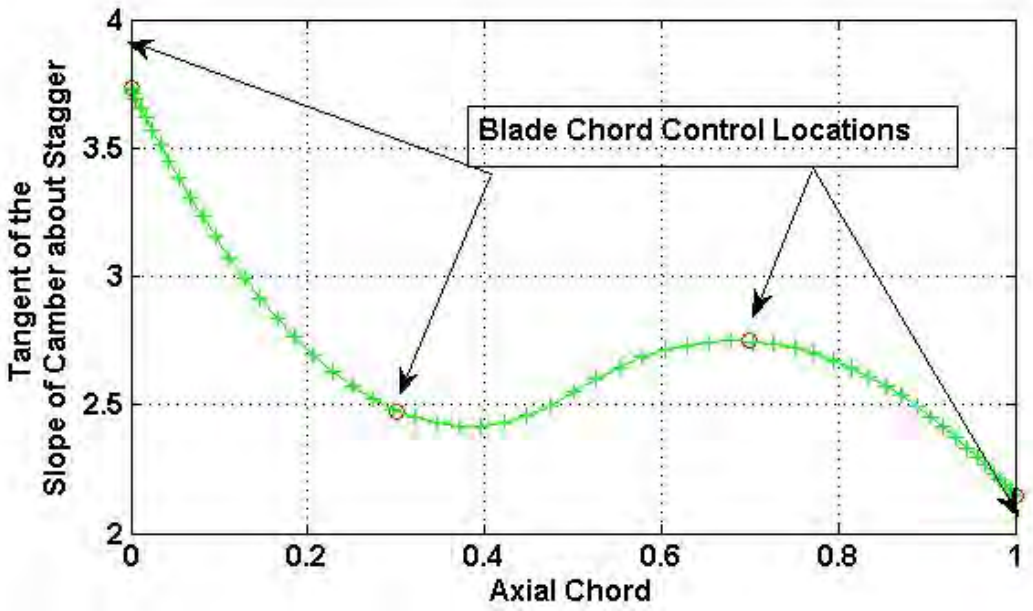

Fig. 10, Third-order spline fit for blade camber line distribution

Blade profile generation continued by using a third-order spline between control points for thickness distribution as shown in Fig 11. The red lines denoting the leading edge and trailing edge blend points.

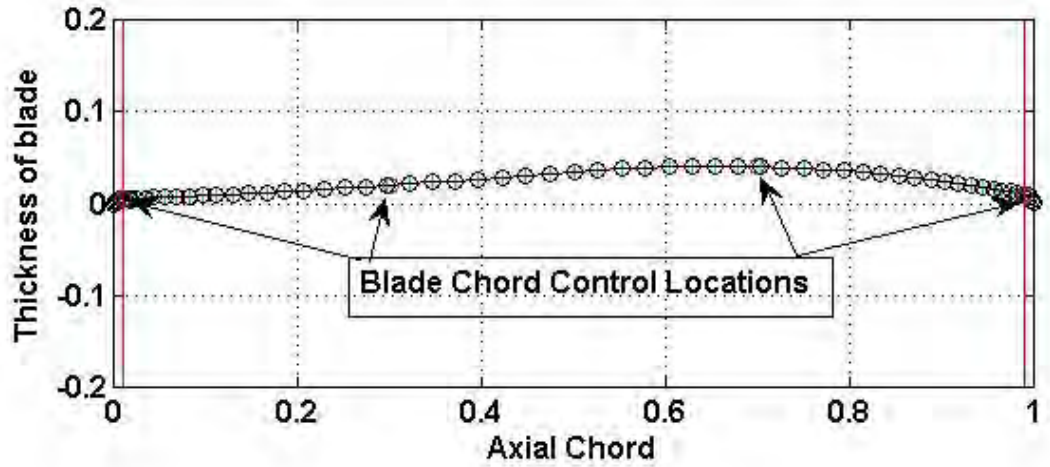

Fig. 11, Third-order spline fit for blade thickness distribution.

A magnification of Fig 11 at the blade leading edge which shows the blend point between the third order spline on the blade and the ellipse of the leading edge is shown in Fig 12.

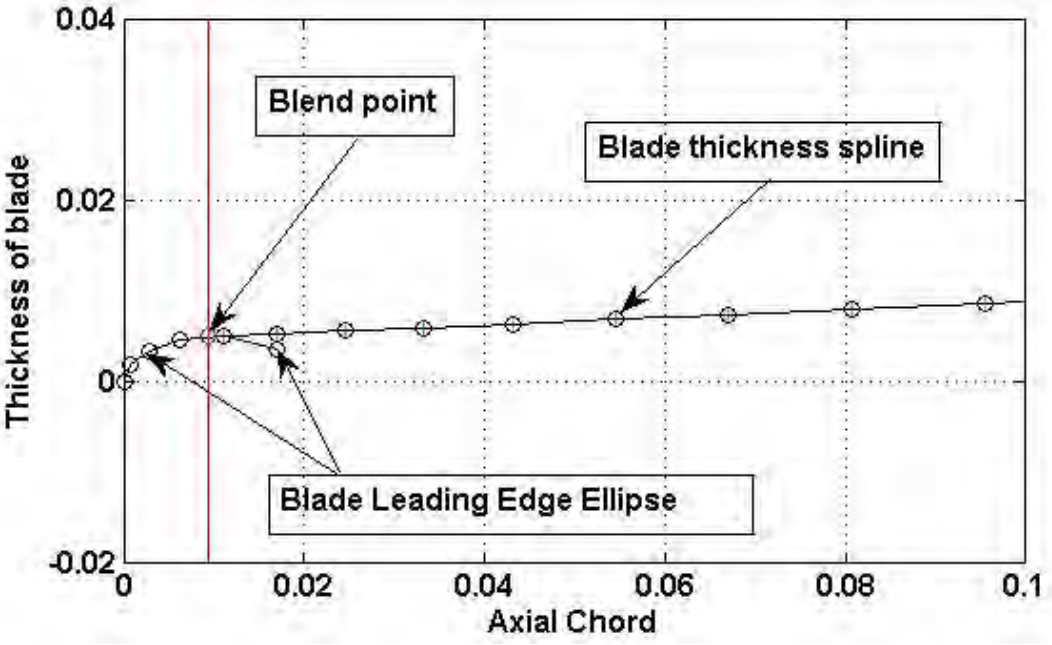

Fig. 12, Blade leading edge: third-order spline fit for thickness.

The thickness distribution accounted for the user-defined blade leading edge and trailing edge ellipse dimensions and eccentricity. Additionally it also ensured blending to the blade surface by matching slopes at corresponding transition points as shown in Fig 13.

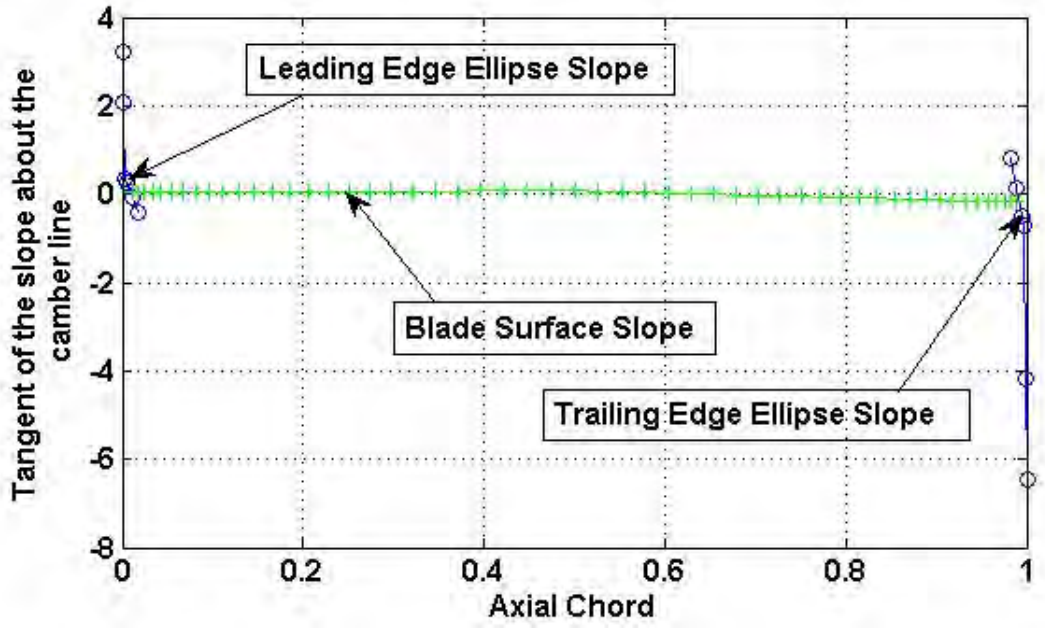

Fig. 13, Blade leading edge and trailing edge slope blending.

Each blade section generated within BladeSect was stacked on its centroid by using the values passed from the polygeom MATLAB script. The polygeom script was derived from Sommer [20] and generated properties (area, x-centroid, y-centroid, perimeter, and area moments of inertia) of a planar polygon. These blade profiles were then passed to SolidWorks for solid model generation of the blade shapes.

Computational Analysis

With solid models generated of the gas-path air wedge, automated numerical performance analysis using CFX within ANSYS Workbench was performed. This was desired in order to produce the data required to generate rotor performance maps. Main_Speedline_Auto continued operation by calling the MATLAB script FluidAnalysis to produce a single speed line from open throttle (zero back pressure) to near stall. The automation terminated when on the current simulation the parameter of interest (pressure ratio, efficiency or power) specified in Main_Speedline_Auto was below the same parameter on the previous simulation or was not a valid number. The cumulative data stored in the spreadsheet was used to map rotor performance graphically.

The computational domain, as shown in Fig 14, extended three axial chord lengths upstream of the rotor (one chord length upstream of the spinner) and two axial chord lengths aft of the rotor. All the design analysis runs were carried out with zero tip gap (TG) and the computational mesh for a single passage had 1.6 million nodes (or 7.2 million elements). Prismatic elements were used as inflation layers on the blade surfaces for 9 layers with a 1.2 stretching factor off the surface. The standard k-epsilon turbulence model was used through out as were high-speed numeric and compressibility corrections to account for correct shock resolution.

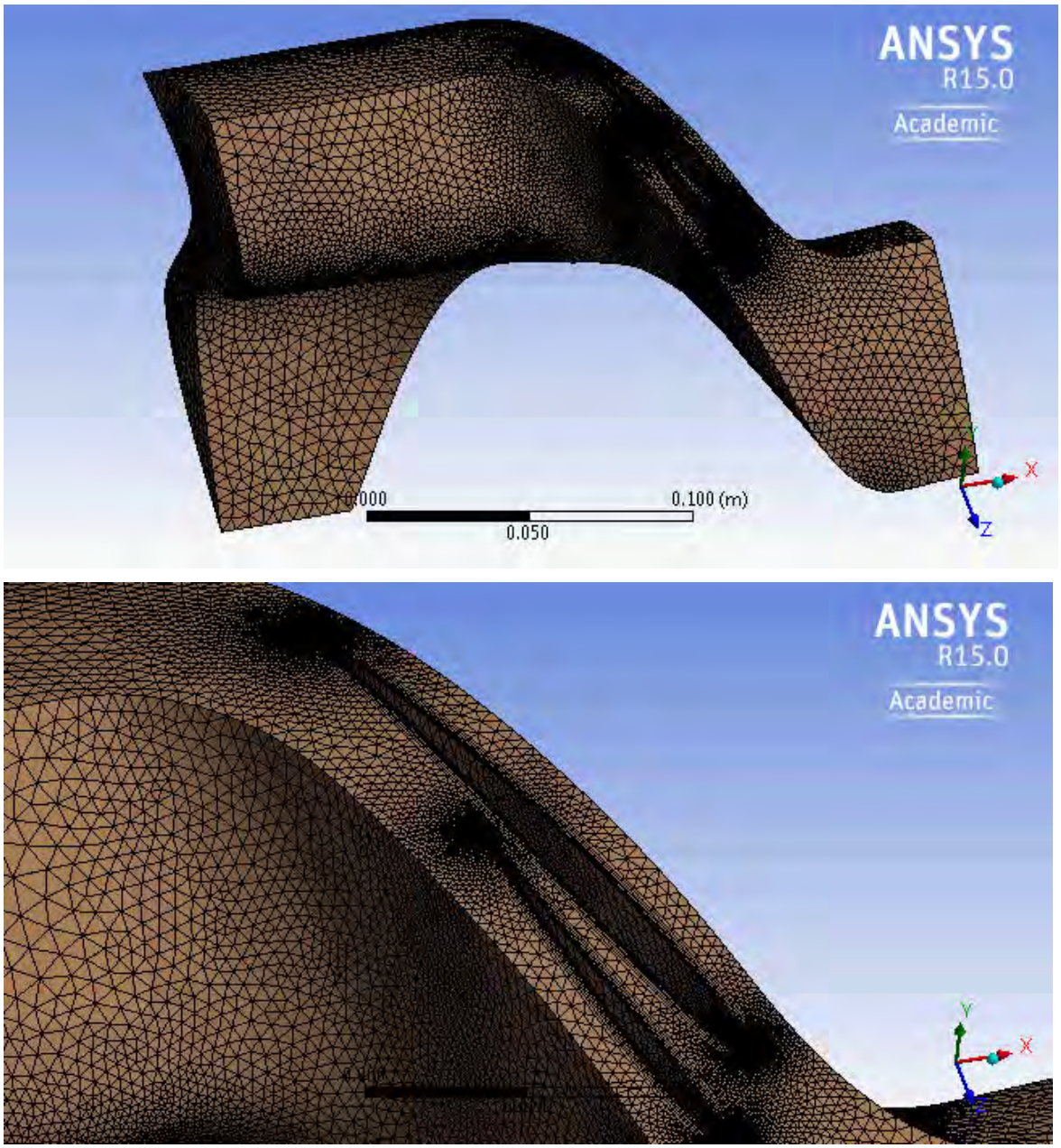

Fig. 14, Design sequence computational domain.

Minimum flow rates were determined when either of the following occurred during the simulation;

(1) less than three orders of magnitude convergence of the residuals
(2) marked drop off of the efficiency
(3) marked drop off of the mass flow rate

Regardless, user interface was till needed to determine three predicted operating range by polling all three of the criteria.

DESIGN OF A TRANSONIC AXIAL COMPRESSOR ROTOR WITH SPLITTER BLADES

The goals and constraints for the Transonic Axial Splittered Rotor (TASR) are listed in Table 1. Additionally a specific weight flow of 195 kg/s-m^2 (40 lbm/s-ft^2) or a mass flow rate of 5.5 kg/sec was targeted.

Table 1. TASR Design Goals and Constraints

Parameter	Goal	Constraint
Rotor Input Power	500 kW	Constrained by available TCR drive turbine output power
Outlet Total-to-Inlet Total Pressure Ratio	1.8 : 1	None
Outlet Total-to-Inlet Total Isentropic Efficiency	80%	None
100% rotor speed	27,000 rpm	None
Casing Diameter	287 mm (11.3 in)	Constrained by existing TCR geometry
Number of Passages	12	None

A blade tip-down design approach was used. The outputs of the previously described combined Sanger method and shock-loss model were used as the starting inputs for the design process. These served as the starting point for good practice human-in-the-loop design improvement.

Four major designs, referred to as Baseline and Spirals 1–3, were explored during the course of the design process and are listed in Table 2. Several iterations were made within each major design study and performance maps for each design and iteration at 100 percent speed (27,000 RPM) were constructed.

The baseline design was derived from the outputs of the combined Sanger method and shock-loss model. The Baseline design solid model was inputted to the Fluid Flow (CFX) module and a mesh was created using Mechanical Model in ANSYS Workbench. Numerically derived total-to-total pressure ratio versus mass flow rate performance map is shown in Fig 15. At 100 percent design speed the predicted peak total-to-total peak pressure ratio was 1.65. Numerically derived total-to-total isentropic efficiency versus mass flow rate performance map is shown in Fig 16. At 100 percent design speed the predicted peak efficiency was 84.9 percent.

Table 2. TASR Design Iterations

Design Iteration	Blade Profile	Splitter Blade Chord	Axial Blade Placement	Splitter Blade Passage Placement
Baseline	Baseline	Splitter blade (SB) chord > 50% main blade (MB) chord	0.00	50%
Spiral 1	Improved Baseline	SB chord = 50% MB chord	0.00	45%
Spiral 2	Improved Spiral 1	SB chord = 50% MB chord	-0.50 - +0.01	40%
Spiral 3	Spiral 2	SB chord = 50% MB chord	-0.02	30 – 35%

Additionally, it was decided that the splitter blade's chord was too long and it resembled a main blade. To ensure the design adhered to the SB concept developed by Wennerstrom [2] a new design constraint was implemented: the SB chord was limited to 50 percent or less of the MB chord.

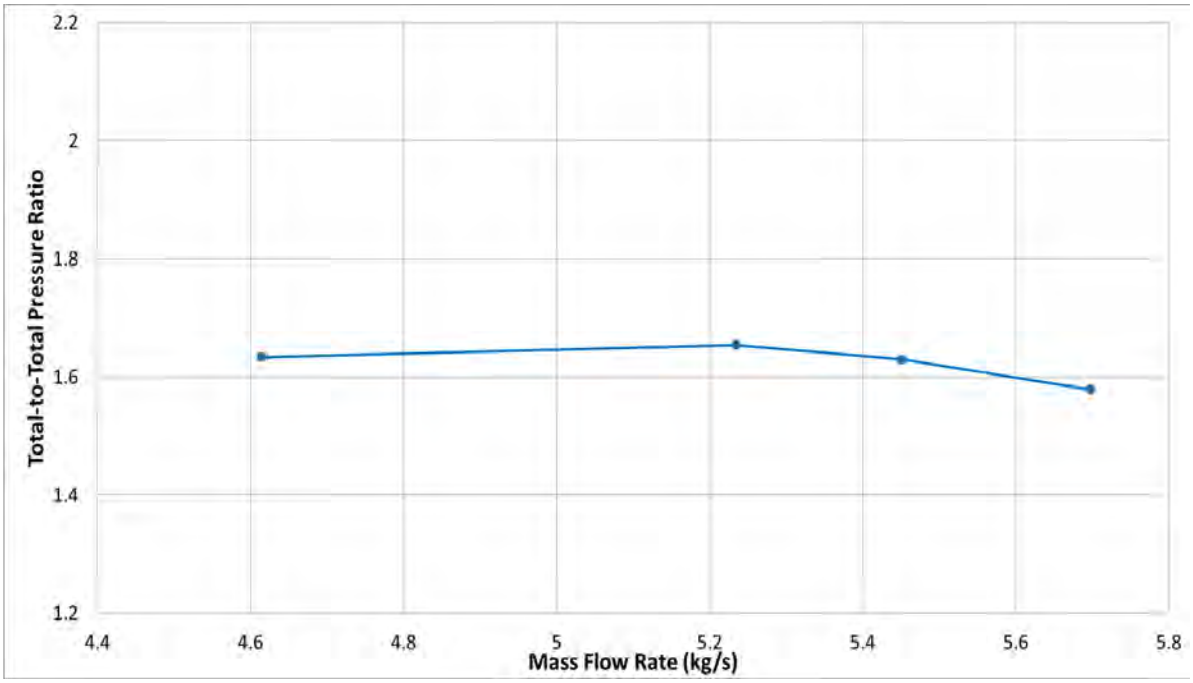

Fig. 15, TASR baseline: Total-to-total pressure ratio map.

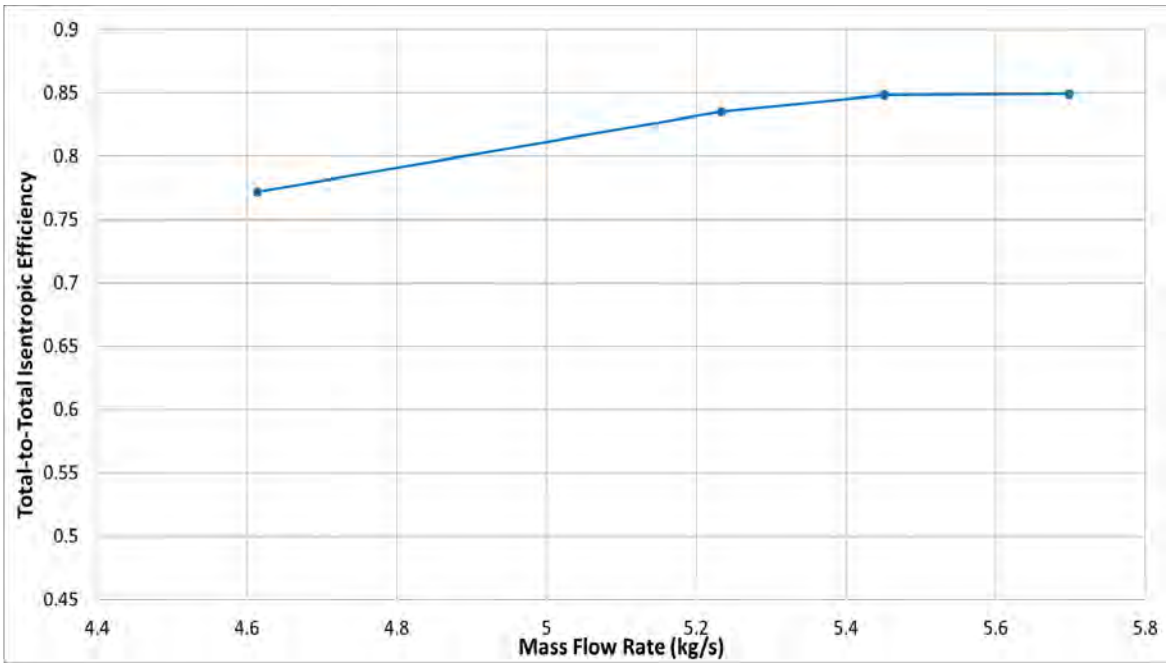

Fig. 16, TASR baseline: Isentropic efficiency map.

The Spiral 1 design implemented the new, self-imposed SB chord design constraint. To counteract the reduction in solidity caused by the shorter SB chord both the MB and SB chords were adjusted, the SB was moved from 50 percent circumferential passage placement (location between the pressure side (PS) and suction side (SS) of the two adjacent MBs) to 45 percent, and both blade profiles were improved. Iterations examined the performance impacts of increased chord lengths on both blades, forward sweep on the MB, and thinner MB and SB. At 100 percent design speed the predicted peak total-to-total pressure ratio was 1.70 and the predicted peak total-to-total isentropic efficiency was 87.7 percent. These performance results also did not meet the TASR pressure ratio design goal outlined in Table 5 and the mass flow rate range was narrower than desired and intuition indicated performance improvements could be achieved by further blade geometry manipulation. The numerically derived total-to-total pressure ratio versus mass flow rate performance map is shown in Fig 17. Numerically derived total-to-total isentropic efficiency versus mass flow rate performance map is shown in Fig 18.

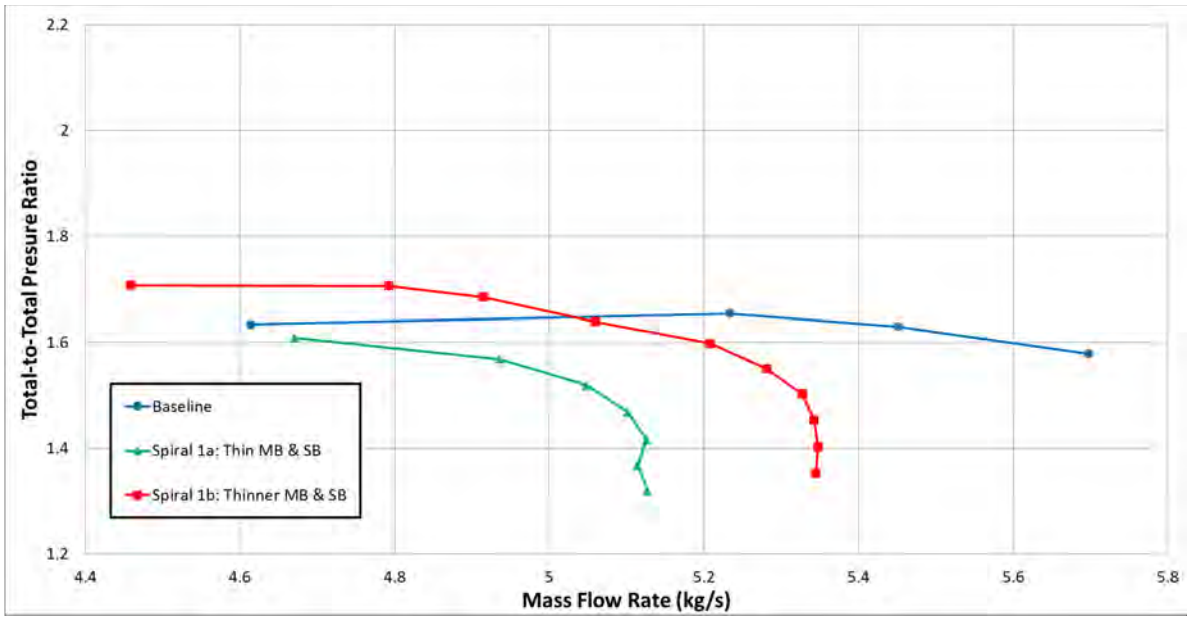

Fig. 17, TASR Spiral 1: Total-to-total pressure ratio map.

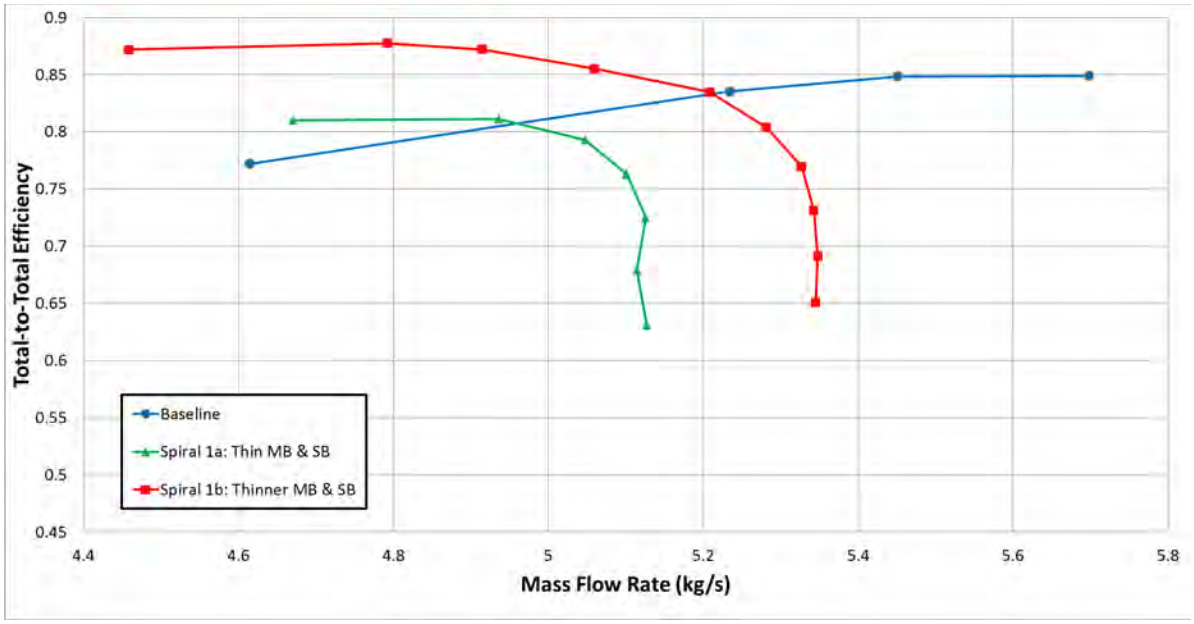

Fig. 18, TASR Spiral 1: Isentropic efficiency map.

The Spiral 2 design improved upon the Spiral 1 blade profile, retained the SB chord restriction, shifted the SB radial placement to 40 percent, and explored the performance impacts of moving the MB and SB axially forward and aft along the hub using the MATLAB script HardCodeBlade input parameter Blade.MasterXShift previously described in Table 1. Varying performance resulted from moving the blades forward and aft. The Spiral 2b design predicted peak total-to-total pressure ratio was 1.83 and the predicted peak total-to-total peak isentropic efficiency was 86.9 percent meeting the design goals of 1.8 and 80 percent

respectively; however, the mass flow rate range was still too narrow. The numerically derived total-to-total pressure ratio versus mass flow rate performance map is shown in Fig 19. Numerically derived total-to-total isentropic efficiency versus mass flow rate performance map is shown in Fig 20.

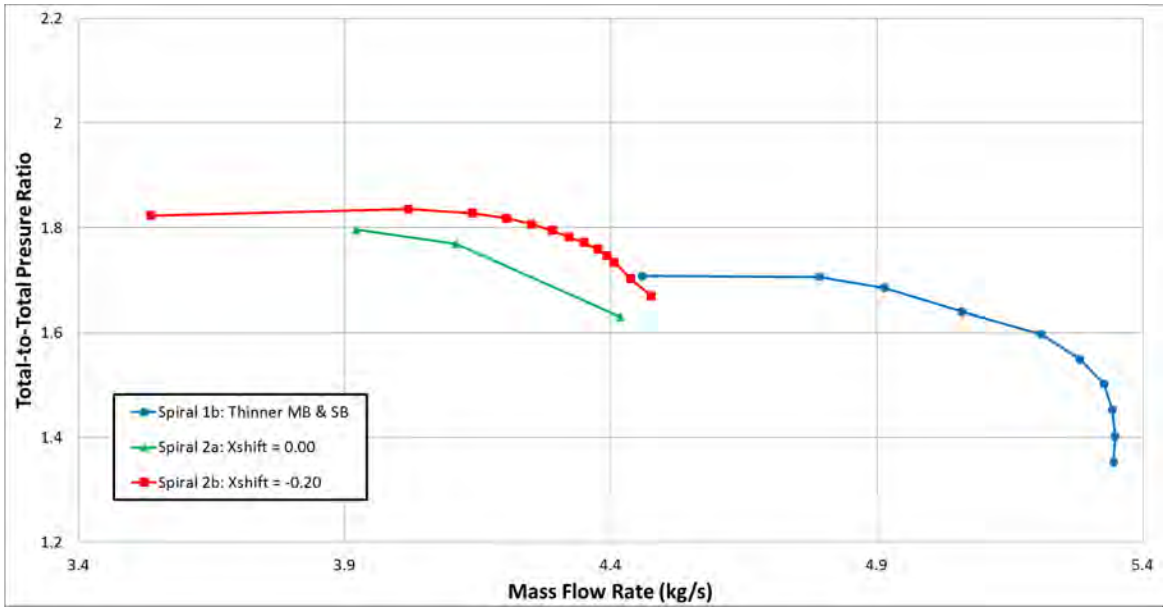

Fig. 19, TASR Spiral 2: Total-to-total pressure ratio map.

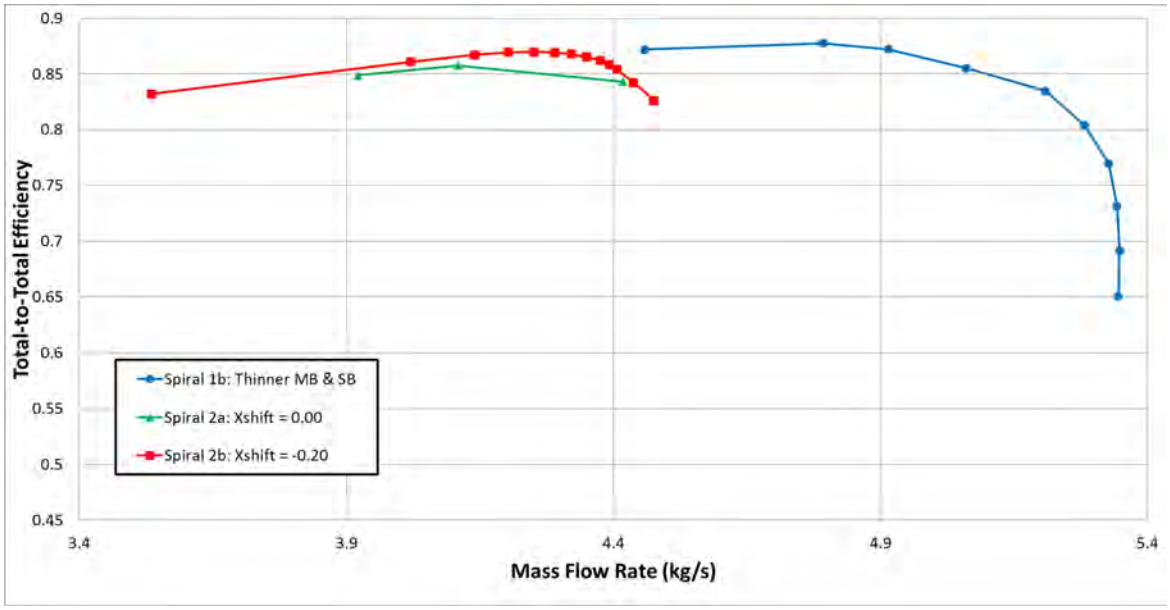

Fig. 20, TASR Spiral 2: Isentropic efficiency map.

The results of this axial blade placement study showed that with Blade.MasterXShift = -0.02 (forward) the rotor produced the best results. The Spiral 3 design froze the geometry of the Spiral 2b design and concentrated on exploring the performance impacts of moving the SB

radially in the passage. Varying performance resulted from moving the SB radially between the adjacent MBs. The numerically derived total-to-total pressure ratio versus mass flow rate performance map is shown in Fig 21. The numerically derived total-to-total isentropic efficiency versus mass flow rate performance map is shown in Fig 22. The results of this SB axial placement study showed that with SB place at 35 percent passage the rotor produced the best results. For this configuration, the predicted peak total-to-total pressure ratio was 2.12 and the predicted peak total-to-total isentropic efficiency was 85.3 percent. The mass flow rate range, Equation (2), was 23 percent.

$$Mass-Flow-Rate-Range=\frac{\dot{m}_{max}-\dot{m}_{min}}{\dot{m}_{max}} \quad (2)$$

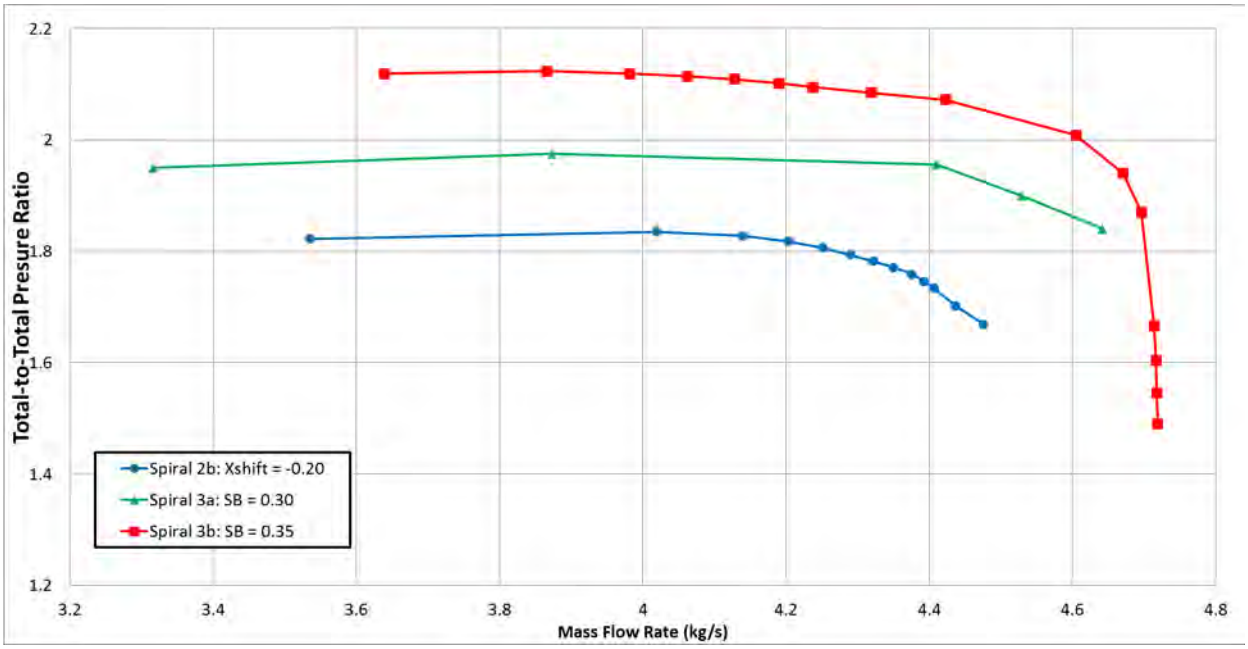

Fig. 21, TASR Spiral 3: Total-to-total pressure ratio map.

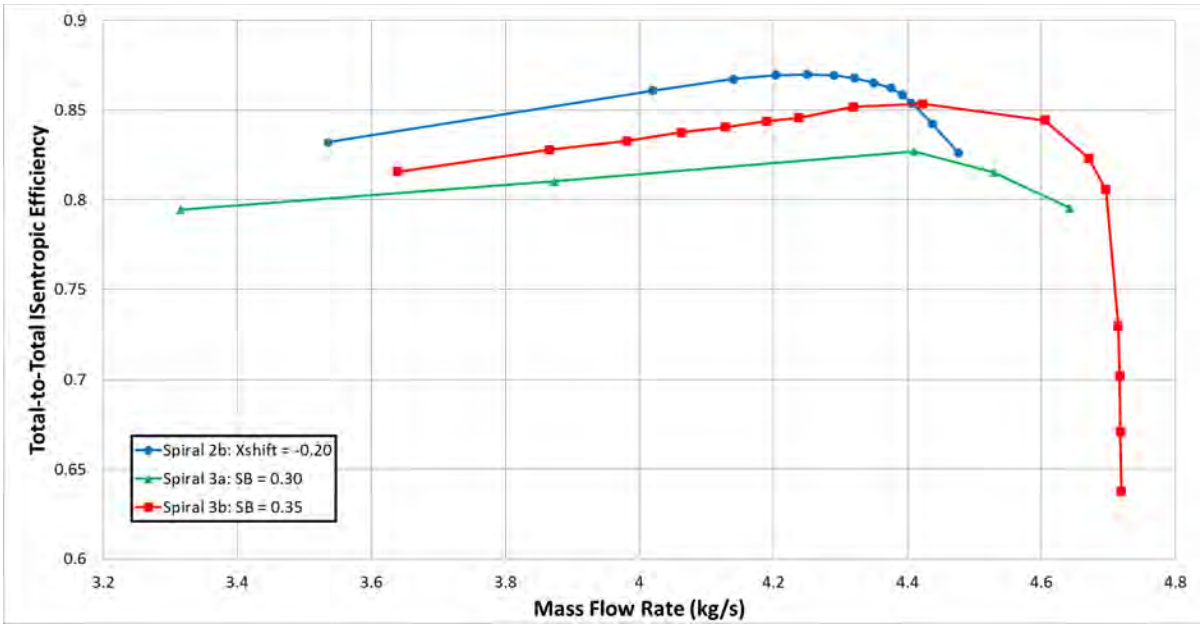

Fig. 22, TASR Spiral 3: Isentropic efficiency map.

A detailed structural analysis was performed on the final blade shapes that were designed during Spiral 3 and slight geometric adjustment had to be made to reduce the stresses at the root of the blades due to centrifugal forces at 30,000 rpm. This was the anticipated maximum speed during stall tests when the rotor would overspeed due to a constant power turbine drive. Full details of the analysis are given in [17]. The final rotor blisk is shown in Fig 23, including the shaft mounting holes and blade-to-disk fillets. The final machined part is shown in Fig 24.

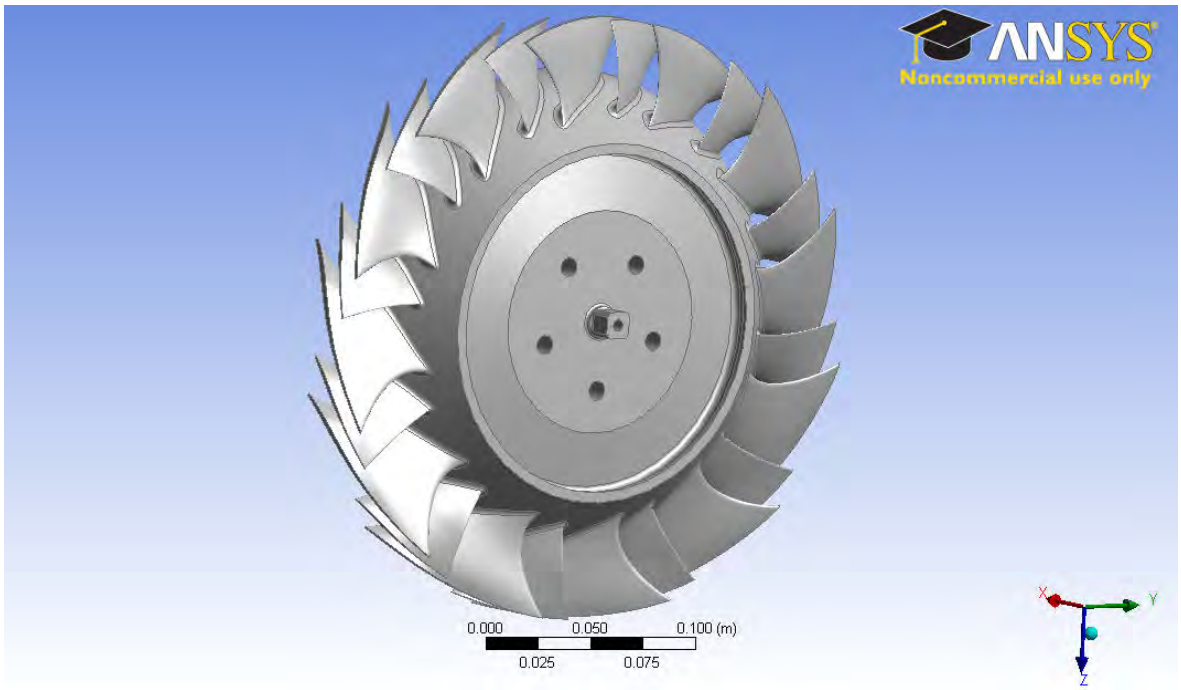

Fig. 23, TASR Spiral 3 structural analysis solid model.

Fig. 24, Final machined TASR blisk

TRANSONIC COMPRESSOR RIG (TCR)

Compressor Installation and Instrumentation

Modifications were made to the rotor-only test section of the TCR to accommodate the TASR as shown schematically in Fig 25. Due to the axially segmented construction of the TCR, the TASR was easily accommodated into the rig by replacing the NPSMF rotor section with a TCR rotor section of identical dimensions with the exception of a wider inner ring of abradable rubber material to accommodate the longer chord of the TASR blades. After assembly the inlet instrumentation was located in axial segment 1 (AS1), the casing transient pressure instrumentation over the rotor were located in axial segment 2 (AS2), and the outlet instrumentation was located in axial segment 3 (AS3). The axial segments are show in Fig 26 and the installed TASR blisk in the TCR is shown in Fig 27.

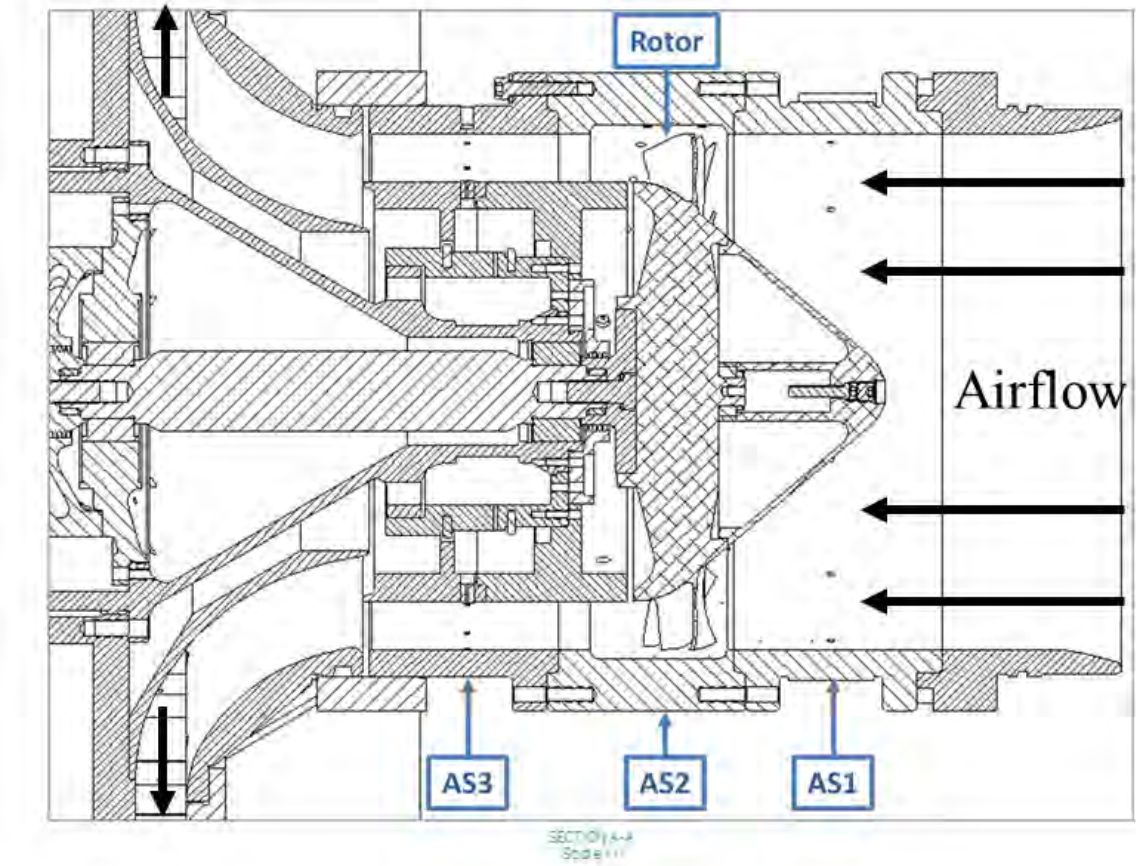

Fig. 25, TCR cross-section with the TASR installed.

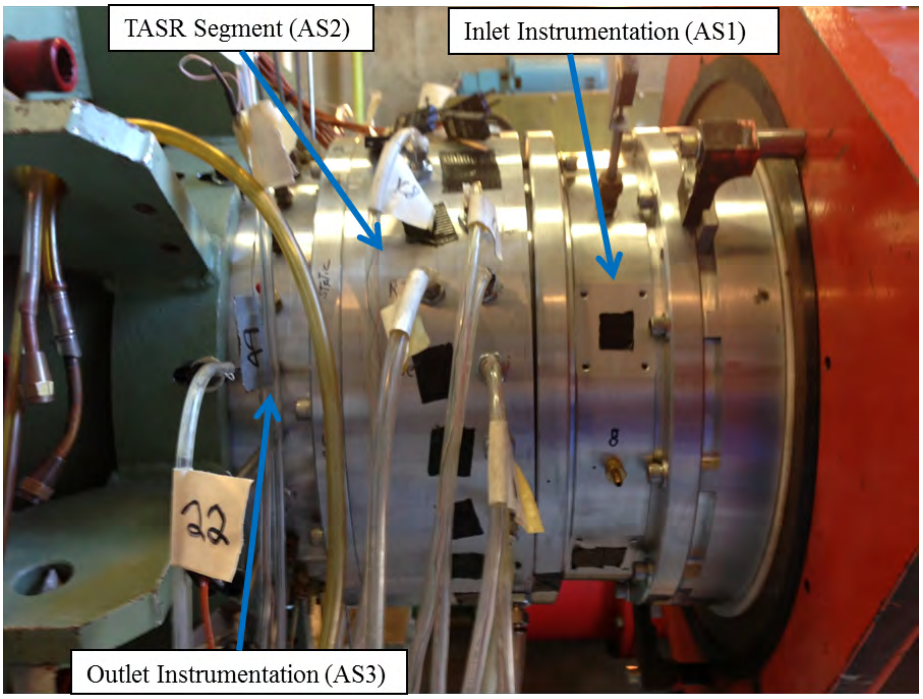

Fig. 26, TASR axially segmented casing.

Fig. 27, TASR blisk and hub section.

The TCR configuration and operation are described in detail by Grossman [18] and are summarized here. The TASR was powered by two opposed rotor, single stage air-operated drive turbines mounted on a common shaft as shown in Fig 28. The drive turbines received supply air from a 12-stage Allis-Chalmers axial compressor capable of providing 2.2 kg/sec mass flow rate at up to 2 atmospheres of gage pressure.

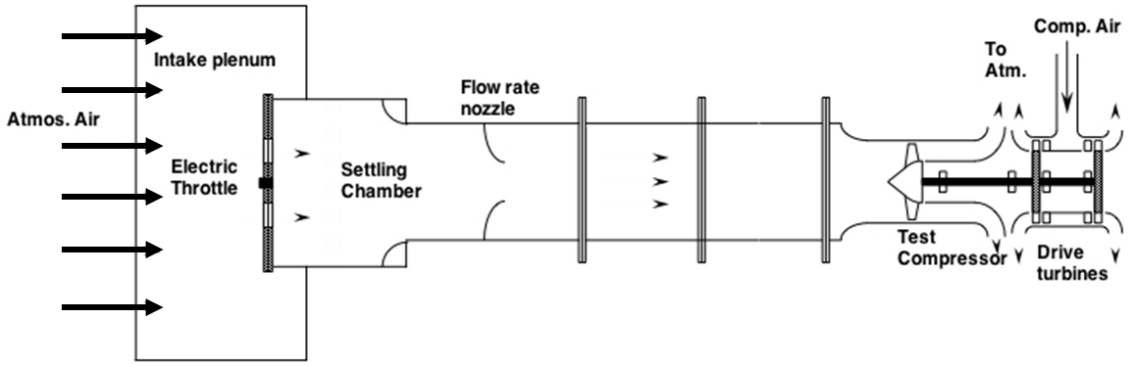

Fig. 28, Transonic Compressor Rig configuration

Experimental Results

Prior to starting the experimental testing of the TASR installed in the TCR increased concern about the stability of the abradable strip material installed in the casing in the blade tip region necessitated the machining of the abradable material to expand the cold-shape tip gap from the planned 0.51 mm (0.020 in) to 0.91 mm (0.036 in). It was predicted that this would negatively impact the experimentally measured performance of the TASR, but the tradeoff was accepted to ensure the integrity of the TASR blisk.

Performance of the TASR was measured at 60 percent, 70 percent, 90 percent, 95 percent, and 100 percent of the 27,000 rpm design speed. The total-to-total pressure ratio, total-to-total isentropic efficiency, and referred power were plotted versus mass flow rate for each specific test speed. From an experimental error analysis the greatest source of error was the mass flow instrumentation equating to a two percent error in the measured mass flow rate. The total-to-total pressure ratio versus mass flow rate is shown in Fig 29. This figure shows the characteristic increase of pressure ratio as the mass flow rate is decreased as a constant rotational speed. The compressor was throttled to stall for all speeds. At 100 percent design speed, the measured peak pressure ratio was 1.69 and mass flow rate range was 7.5 percent. At 70 percent design speed, the measure peak pressure ratio was 1.33 and the mass flow rate range was 18 percent.

Before proceeding with the comparison, it is important to recall that the numerically derived predicted performance was modeled using a TG of 0.25 mm (0.010 in) but the TASR was experimentally tested with a cold, non-deformed shape TG of 0.91 mm (0.036 in). Additionally, the numerical simulations performed in this study were predictive and time did not permit refining the simulations to try to match the predicted numerical performance to the measured experimental performance. As predicted, with a larger TG, the experimental data

shows a reduced peak pressure ratio and increased mass flow rate at all operating speeds. At 100 percent design speed the predicted peak pressure ratio was 1.92, but the measured peak pressure ratio was 1.69. The predicted mass flow range was 6.0 percent and the measured mass flow range was 7.5 percent. Although the measured pressure ratio was lower than predicted the measure flow range was higher than predicted. This increased flow range will result in an increased operability range if used in an actual engine.

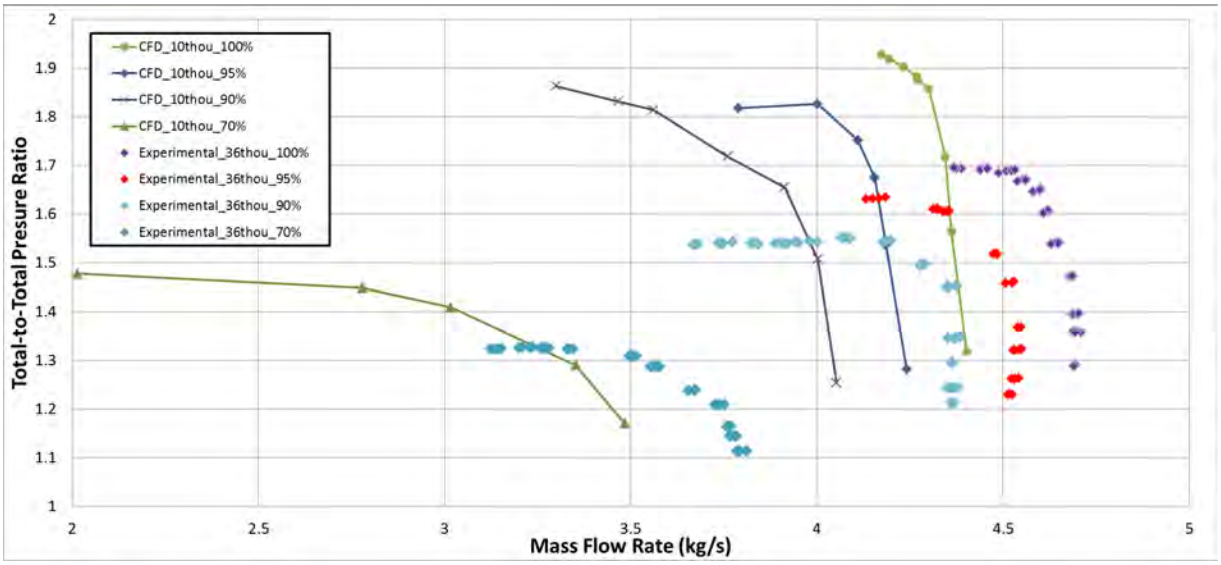

Fig. 29, TASR experimentally versus numerically determined total-to-total pressure ratio map.

Fig 30 shows the numerical results for total-to-total isentropic efficiency plotted on the map of the experimentally determined data. Again, the larger TG reduced performance and reduced the peak efficiency at all operating speeds but increased mass flow rate. The predicted peak efficiency for 100 percent design speed was 80 percent but the measured efficiency was 72 percent. Again, the experimental performance maps and the numerically determined maps matched in characteristic, in that although the pressure ratio and efficiency were down due to the increased tip leakage the flow range was similar. The experimental flow range (at 0.91 mm tip gap) was slightly larger than that predicted at the analyzed 0.25 mm (0.010 in) tip clearance.

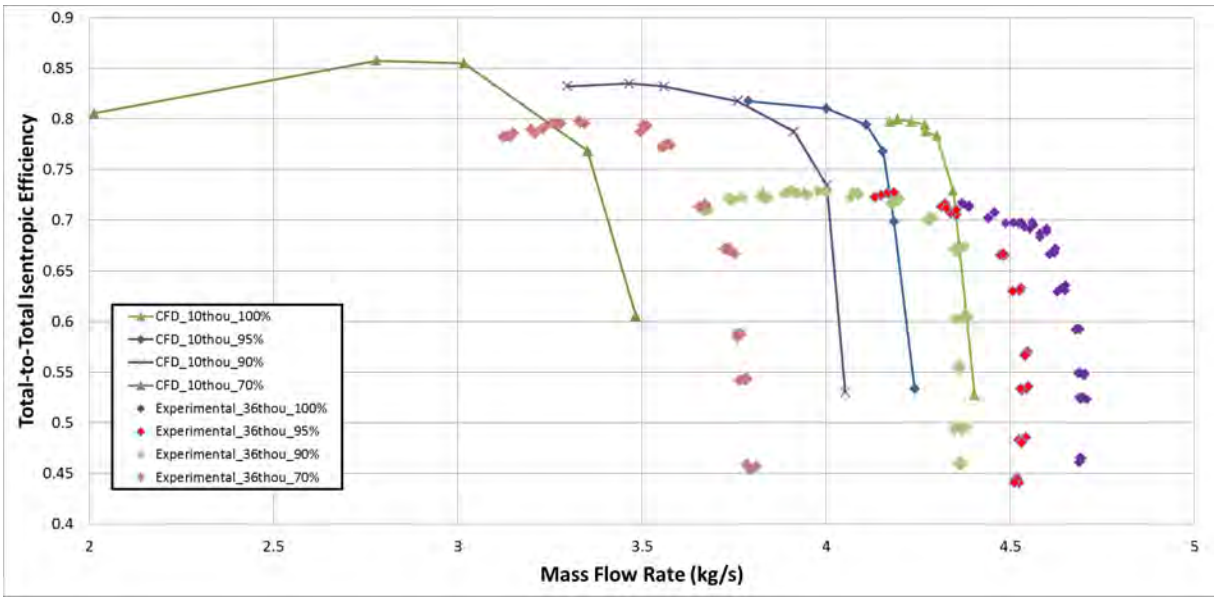

Fig. 30, TASR experimentally versus numerically determined isentropic efficiency map.

The power absorbed by the compressor versus mass flow rate for the range of operating speeds is shown in Fig 31. This is the corrected mass flow rate and it should be noted that the actual power absorbed by the TASR was less due to the upstream throttling. The peak power actually absorbed by the compressor at each operating speed is lower than presented. For example, at 100% design speed the measured corrected peak power absorbed was 425 kW. The measured uncorrected peak power absorbed was 317 kW. The corrected power was calculated using equation (3). The map for each operating speed is shifted to a higher mass flow rate range as predicted due to the increase in TG.

$$HP_C = C_p \dot{m}\left(T_{03} - T_{01}\right) \qquad (3)$$

where C_p is the specific heat of the air and $\dot{m}$ is the corrected mass flow rate.

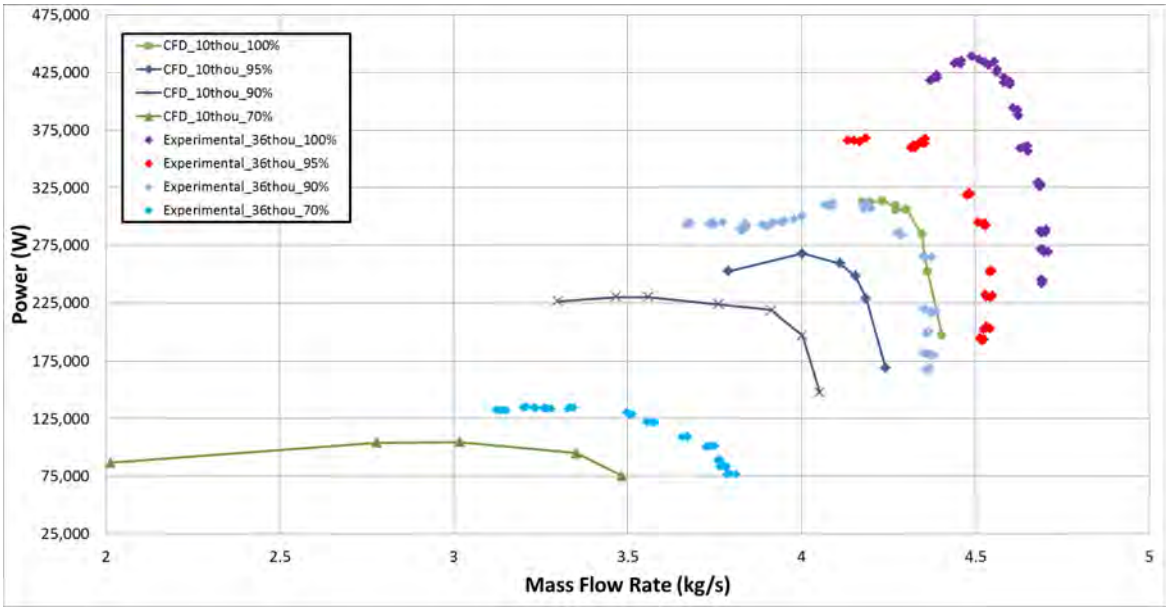

Fig. 31, TASR experimentally versus numerically determined power map.

Utilizing the MATLAB code developed by Londono [19] the unsteady Kulite data of the casing pressures was analyzed for the 100 percent design speed at the near-stall condition resulting in the contour plot shown in Fig 32. In this figure a strong oblique shock is originating from the leading edge (LE) of the splitter blade (SB) and a weaker oblique shock is originating from the LE of the main blade (MB). The casing contour plot extracted from the numerically derived performance data at 100 percent design speed in the near stall condition is also shown.

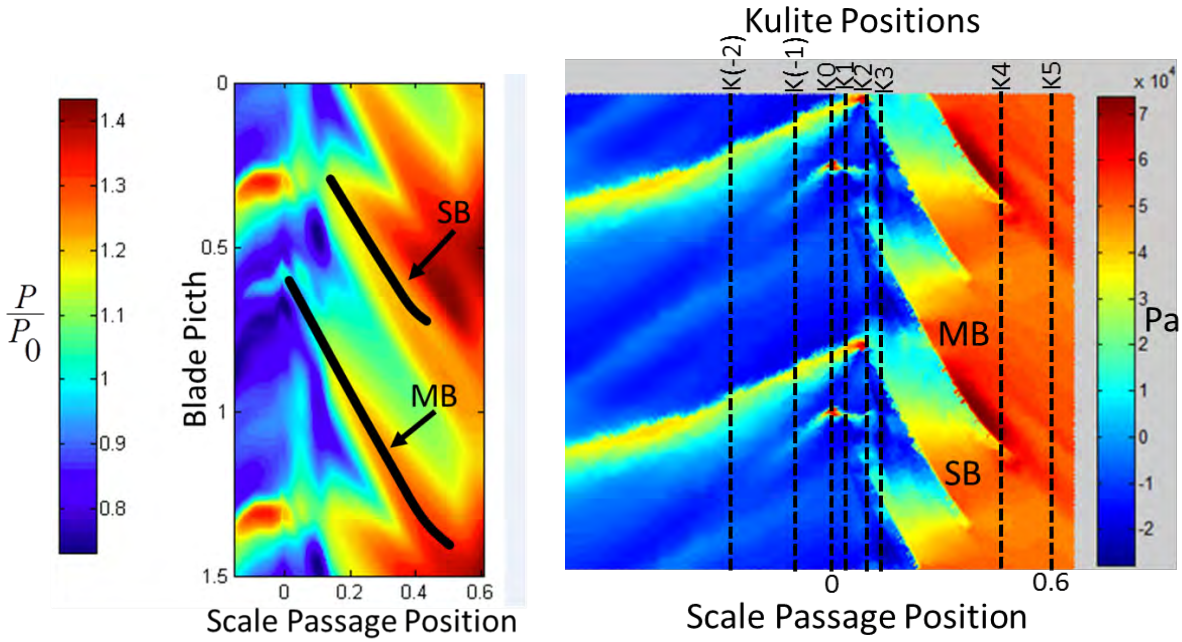

Fig. 32, TASR 100 % speed near-stall experimental (left) and computational (right) casing contour pressure plot.

Comparing these figures the experimentally derived contour plot for the same conditions shows similar flow field characteristics to the computational results. A strong oblique passage shock wave can clearly be seen starting in the SB LE tip region and a smaller oblique shock can be seen originating from the MB LE tip region. The combination of these shock waves inhibits the fluid flow creating flow blockage into the passage and setting up a stall condition.

Further a tip gap variation study was performed by machining the casing to different diameters as shown in Table 3. The absolute cold tip gaps used are 0.99 mm, 0.76 mm and 0.53 mm and are used as the reference values through this study. As can be seen the rotor diameter does not change while the casing diameter is machined to the desired diameter.

Table 3. Cold rotor, casing and tip gap sizes

Cold Tip Gap [mm] (in)	**0.99 (0.039)**	**0.76 (0.030)**	**0.53 (0.021)**
Inlet/Outlet Diam [mm] (in)	287.22 (11.308)	Same	Same
Casing Diam. [mm] (in)	289.02 (11.378)	288.54 (11.360)	288.09 (11.342)
Rotor Diam. [mm] (in)	287.02 (11.300)	Same	Same
Tip Gap/Blade Height [%]	2.6%	2.01%	1.40%
Tip Gap/Blade Chord [%]	1.28%	0.98%	0.68%

It must be noted that at the speeds being tested rotor deformation or the so-called ‘hot’ shape geometry does affect the tip gap significantly. A very simple mechanical deflection analysis was performed using the software package “Ansys Mechancial” to obtain radial deformation of the tips of the blades at 27 000 rpm.

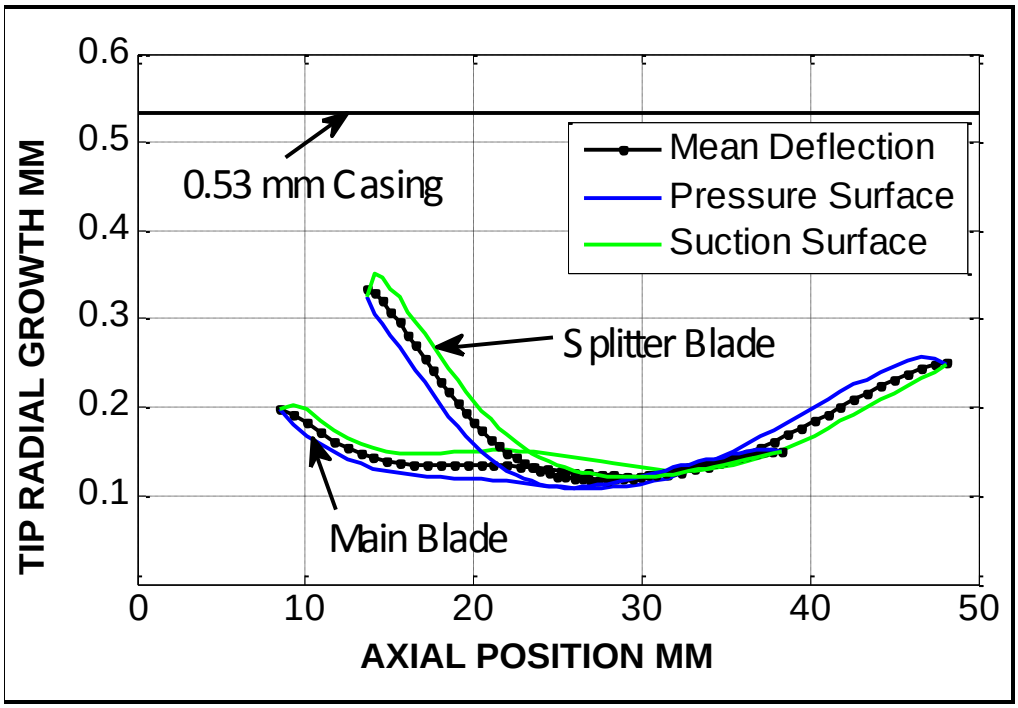

Fig. 33, 10% Speed radial blade growth

Fig 33 shows the radial growth of the main and splitter blades respectively. The zero position on the y-axis is the un-deformed or cold blade-tip position. Also plotted is the 0.53 mm casing position corresponding to the smallest tip gap. It can be clearly seen that the variation in the gap is not constant. In the case of the main blade the leading and trailing edges have the largest deflections due to the longer chord at the casing. In the case of the splitter blade the stacking method used leads to the largest overall radial deformation at the blade leading edge.

Table 4 lists the approximate hot tip gaps compared to the cold ones. It can be seen that as a fraction, the decrease in gap is significant. This gap is calculated using the median values of blade growth of the main and splitter blades taken from Fig 33. The average of these two medians is then used to calculate the approximate hot tip gap.

Table 4. Deformed (hot) tip gap sizes

Cold Tip Gap [mm] (in)	**0.99 (0.039)**	**0.76 (0.030)**	**0.53 (0.021)**
Approx. Hot Tip Gap [mm] (in)	0.79 (0.031)	0.56 (0.022)	0.33 (0.013)
Average Median Growth [mm] (in)	0.20 (0.008)	Same	Same
Main blade median growth [mm] (in)	0.18 (0.007)	Same	Same
Splitter blade median growth [mm] (in)	0.23 (0.009)	Same	Same

Fig 34 shows the turbulence intensity of the rig inlet as measured by Payne [20] against the mass flow. A TSI 1212-20, 20 μm, hotfilm probe was used. This was measured for a different rotor, so the speed lines do not correspond to those in this study but the rig inlet geometry has not been modified. The medium turbulence intensity is near 2.25%. The inlet mass flow is accurate and measured at two locations to ensure that no leakage takes place.

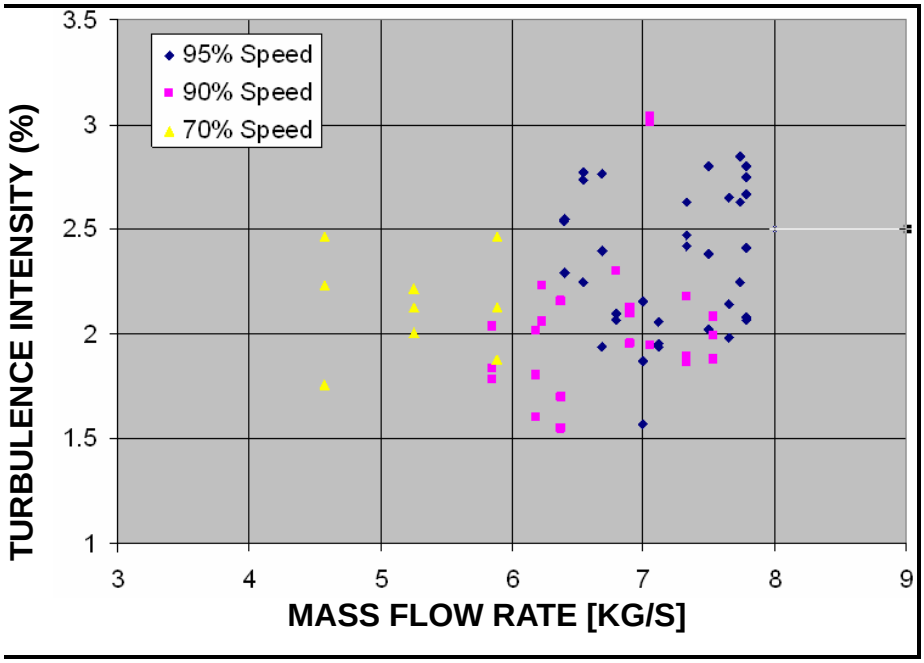

Fig. 34, Rig inlet turbulence intensity

Performance Maps

A wide range of operation was tested in the current program. As noted previously the intention is to provide a data set that is representative of differing compressor stages within a gas-turbine engine.

Table 5. Rotor tip speeds and Mach numbers tested

Speed-line [%]	60	70	80	90	95	100
Tip-speed [m/s]	243.5	284.0	324.6	365.2	385.5	405.8
Tip-Mach [-]	0.71	0.83	0.95	1.07	1.13	1.19

Table 5 gives values of the tip speed and Mach numbers tested. The front stages usually have a smaller ratio of tip-gap to blade height than the aft core stages. In addition the front stages are usually operating in the transonic regime while the rear stages operate sub-sonically due to the temperature gain through the compressor stages.

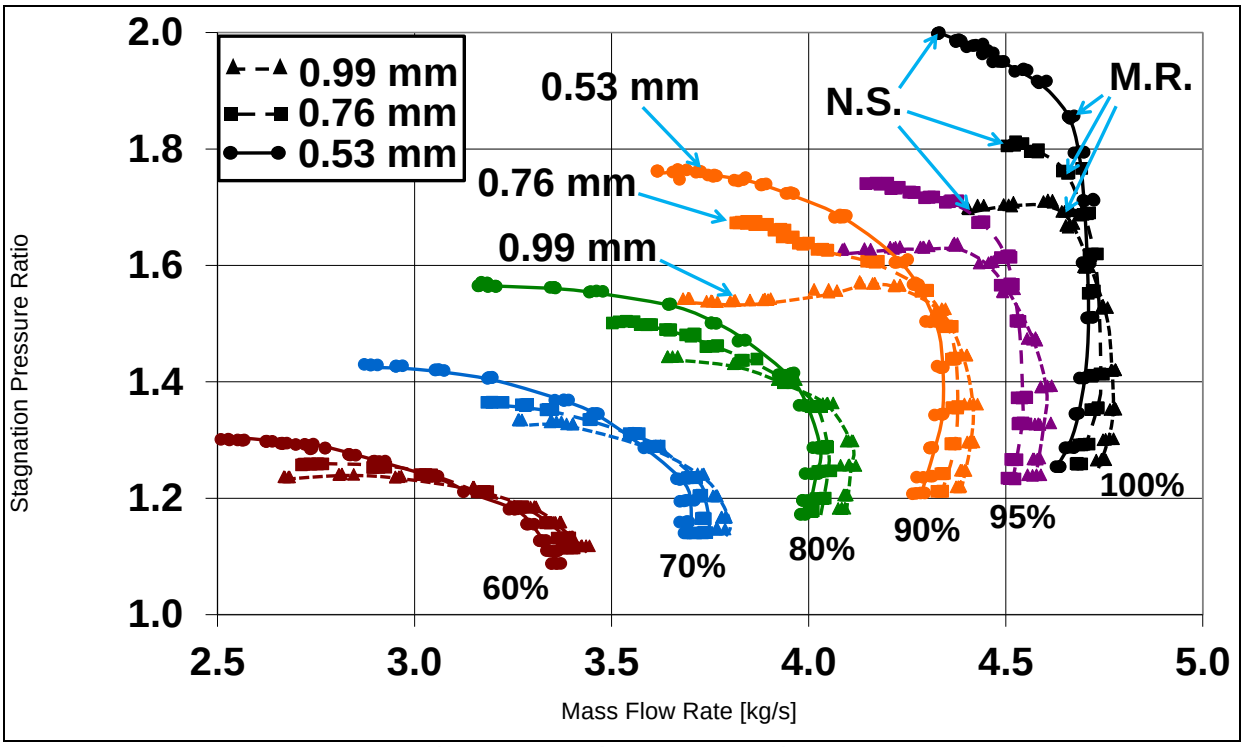

Fig. 35, Stagnation pressure ratios.

Figure 35, shows the stagnation pressure ratios for varying tip gaps from subsonic to transonic operation with the corresponding tip Mach numbers and speeds shown in Table . Once the relative velocities are taken into account, 80% speed is near sonic at the tip while the rest are firmly supersonic. The transonic test rig in use for this study has an efficient diffuser, which allows testing of the chocked flow region with its typical vertical characteristic when operating in the transonic region. These results are left in the main performance maps for completeness but may not be in the typical operating range of a compressor.

Full Open Throttle Operation

As mentioned this mode of operation would not be commonly encountered in an operation engine due to the low efficiency operation at these setting as can be seen in Fig. 35 and Fig. 36. However due to the interesting flow phenomena and the potential to improve simulations by being able to capture this characteristic it is discussed here. For the full open throttle operation it can be seen that the mass flow rate is higher for the larger tip gaps for all speeds lines. This is to be expected as the effective area of the fan passage has been increased. When the pressure ratio is low, flow is entrained in the tip gap thereby increasing the overall mass flow rate. As the throttle on the experimental rig is closed and the compressor moves up a speed-line a crossover point occurs and the mass flow decreases with increasing tip gap due to leakage flow through the tip gap. At 60% and 70% speeds the slope the speed-line is unremarkable with the mass flow decreasing with increasing pressure ratio.

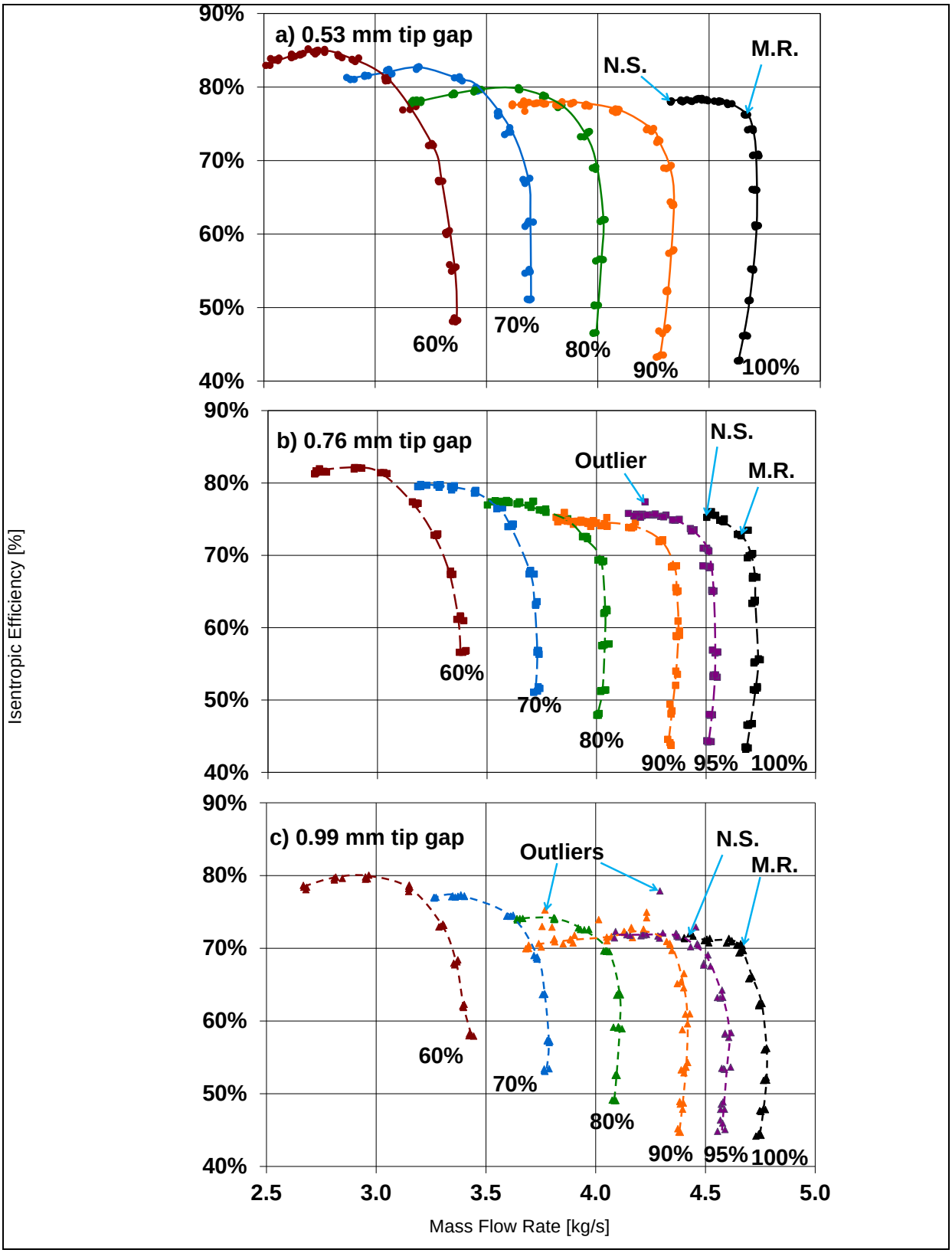

Fig. 36, Isentropic efficiencies.

For 80% speed and above the speed-lines become less conventional; the mass flow initially increases with increasing pressure ratio. This was initially predicted during the design phase and at that stage considered to be an error in the simulation, however the experimental results showed that the predictions were correct. While it is beyond the scope of this study to discuss this in detail it appears to be due to the changing shock structure as the pressure ratio increases. This explains why for the subsonic cases it does not appear. Also recall that the flow through the blade is supersonic at low pressure ratios with the final normal shock being at the trailing edge of the blade meaning there is not sonic throat within the blade passages. The absolute efficiencies for the open throttle operation are extremely low as shown in Fig. 36.

Mid-Range to Near-Stall Operation

The mid-range (M.R.) operation points and region are marked on Fig. 35 and Fig. 36 for 100% speed. The mid-range points were chosen based on their efficiency values being the first point where the compressor begins to operate along a traditional operating line with mass flow decreasing as the pressure ratio increases. It is postulated that with the splittered design the rotor may appear to behave as two separate systems. This postulation would appear to be correct in observing the behavior of the operating lines in the transonic region. They initially are very vertical and then at around the mid-range operating region begin to behave in a more traditional way with the mass flow decreasing as the pressure ratio increases. The design process focused on improving the mid-range to near-stall operation leading to this type of behavior (Fig. 36). The shock structure's movement from the rear to the front of the rotor during throttling in a splittered rotor is more complex than for a standard single blade-type rotor.

In Fig the effect of a larger tip gap can be seen by the reduction of the stalling pressure ratio when operating above the mid-range point. For the very large tip gap of 0.99 mm the near stall pressure ratio is actually decreases towards stall for the 90%-100% speed-lines. Fig shows that the efficiencies decrease significantly for increasing tip gaps in all cases.

Near-Stall Operation

The near-stall (N.S.) operating points are the last stable operating points before a very small closing of the throttle caused the compressor to stall. Some interesting differences are observed in the behavior of the compressor near to stall for the differing tip gaps.

The largest operating range is found for the smallest 0.53 mm tip-gap case. At 100% speed a 1.99 stagnation pressure ratio is the highest measured for this rotor. For this small tip-gap case the stall occurred immediately after a final small movement of the throttle and it was thus simple to determine the operating range.

For the larger 0.76 mm tip gap the range of operation is smaller as is usually expected and is true across all speed-lines. Some instability was observed during the 95% operation near to stall as can be seen in the single outlier point in Fig. 36b. For the two larger tip-gaps when operating near to stall, a short unexpected single surge cycles into and out of stall occurs. Sampling sometimes takes place during these events and as the temperature and pressure measurements are sampled sequentially erroneous performance values are calculated. They are left in the figures as measured for completeness.

For the very large tip-gap case shown in Fig. 36c many more of these outlier points can be seen. In Fig. 35 it can be seen that for the 90%-100% speed-lines the operating range is wider which was unexpected. In the 90% case no stall actually occurred during testing as a loud single note harmonic was heard from the compressor. This increases markedly in volume as the throttle is closed and so a decision was made not to operate the compressor in this condition for fear of damaging the rotor. For the 95% and 100% cases the short single stalls were more prevalent which leads to difficulty in determining the exact last stable operating point.

Effect of Efficiency of Tip Clearance

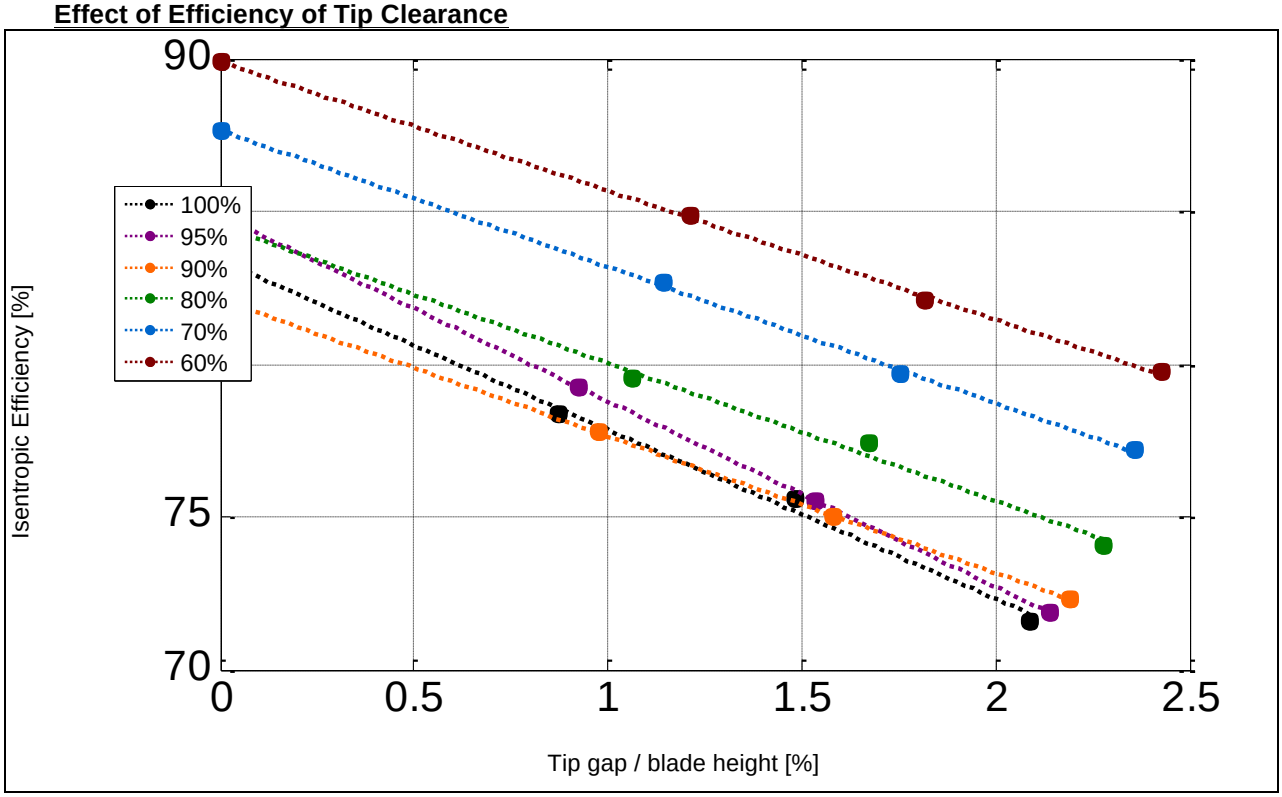

Fig. 37, Maximum efficiencies as a function of tip gap.

An investigation of the effect of the tip gap on the efficiency is now undertaken. Figure 37, shows the absolute value of the maximum efficiency measured against the non-dimensionalized tip gap. The tip gap-to-blade height ratios were calculated using the data from Table . For the tip gaps at lower speeds the usual quadratic relationship between deflection and rotor speed was used. The zero tip-gap case is extrapolated from the speed line data using a linear function. The use of a higher order polynomial with only three data points was not considered prudent. As can be seen the overall trend is similar across the speed-lines.

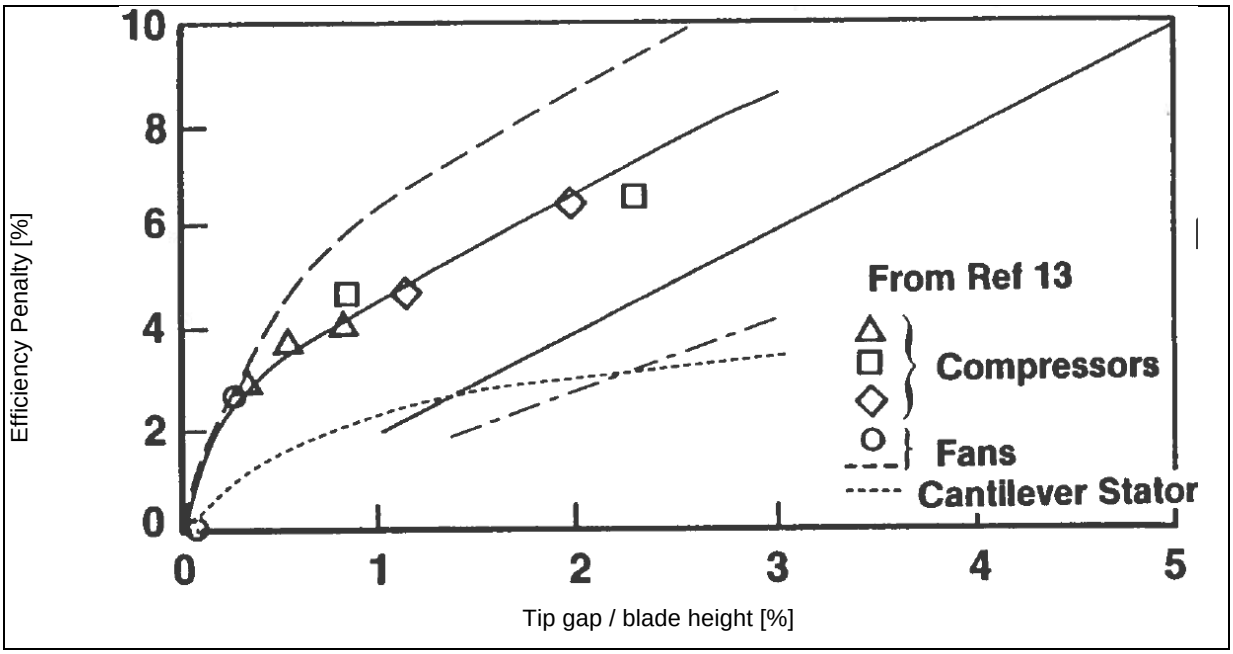

Fig. 38, Efficiency penalties, Wisler [23].

Figure 38 presents data from Wisler [21] based on experimental measurements. It shows the expected decrease in efficiency versus the non-dimensionalized tip gap. According to this work, fans appear to be more sensitive to the tip gap than compressors. It must be noted that the x-axis for this figure covers a wider range of tip-gap heights than in Fig. 37 and Fig. 39.

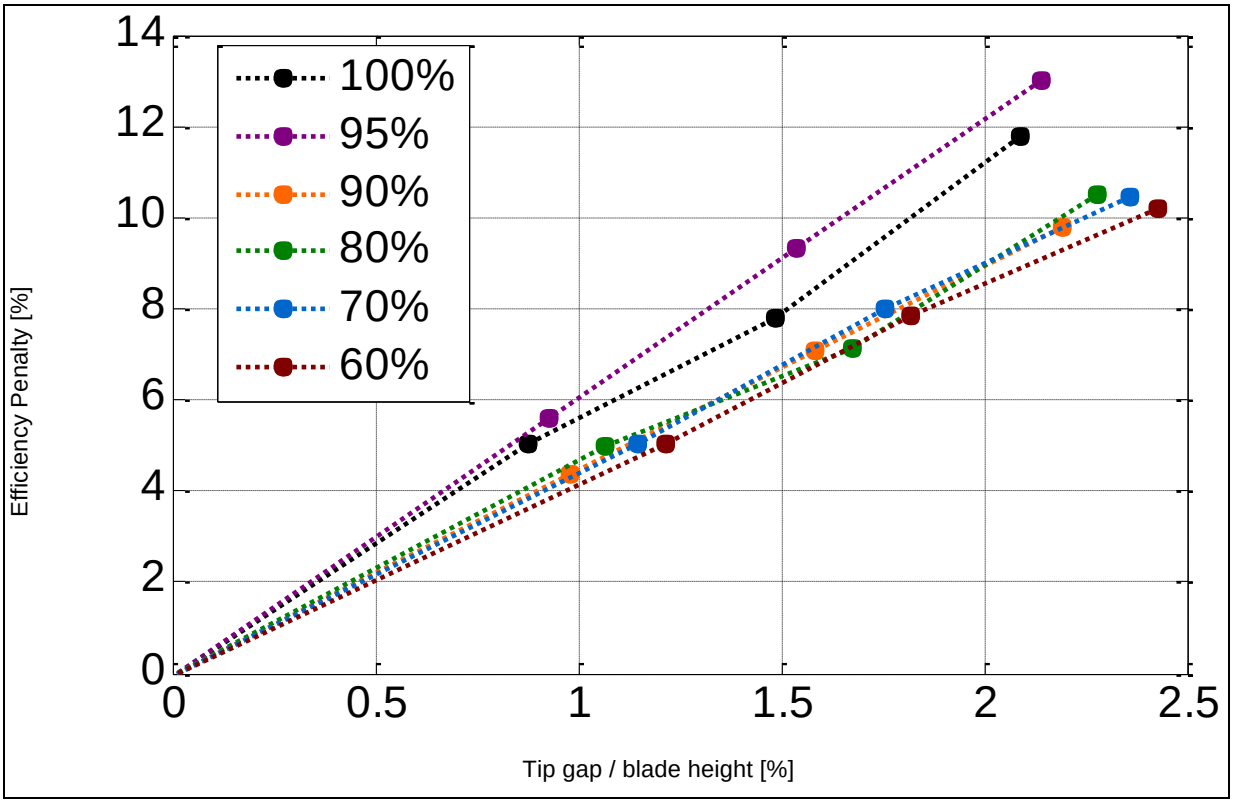

Fig. 39, Efficiency penalties for splittered rotor.

Figure 39 shows the same type of data as that from F but for the current splittered rotor. Comparing the data set to that of Wisler [21] it can be seen that the splittered rotor has the steeper penalty curve characteristic of a fan. For the range of tip gaps investigated however no leveling out of the penalty curve was seen with the lines appearing to be linear until some further point. Looking at the data from the splittered rotor it can be seen that there is a good correlation in the penalties from 60% to 90% speed. At 95% and 100% speeds steeper curves are found. This is presumably an effect of the stronger shocks that are present due to the supersonic flow.

Exit Profiles

Figure 40 shows the exit stagnation pressure ratio profiles for the three tip gaps tested for mid-range (a) and near-stall (b) operation. Data points are located at the location of the downstream stagnation pressure and temperature probes. The overall pressure ratios increase with decreasing tip gaps with a noticeable increase in the pressure ratio at the blade tip for the smallest gap for both cases. In Fig. 40 b) for the near-stall case the influence of the tip gap is large with a significant increase in the pressure ratio. This indicates that the rotor tip is the location of the stall.

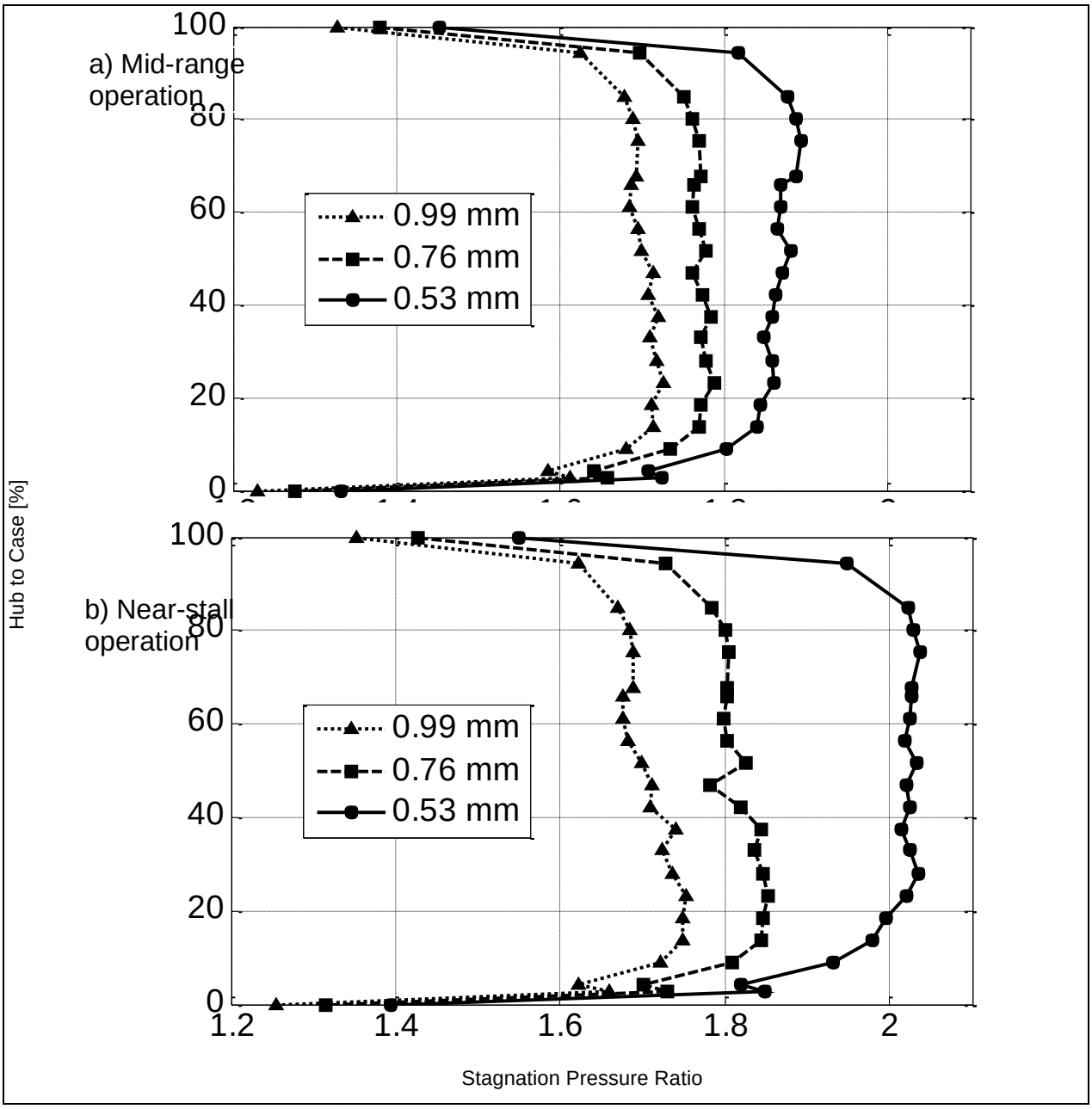

Fig. 40, 100% speed stagnation pressure ratio profiles.

Figure 41 shows the exit stagnation temperature ratio profiles for the three tip gaps tested for mid-range (a) and near-stall (b) operation. Again the data points reflect the position of the stagnation temperature probes.

As with the pressure ratio's profiles there is a similar trend of increasing temperature ratios with decreasing tip gaps. While there is less resolution in the data due to fewer temperature probes being used a marked increase in the temperature ratio downstream of the blade tips can be seen. As expected there is an increase in the temperature ratio as stall is approached.

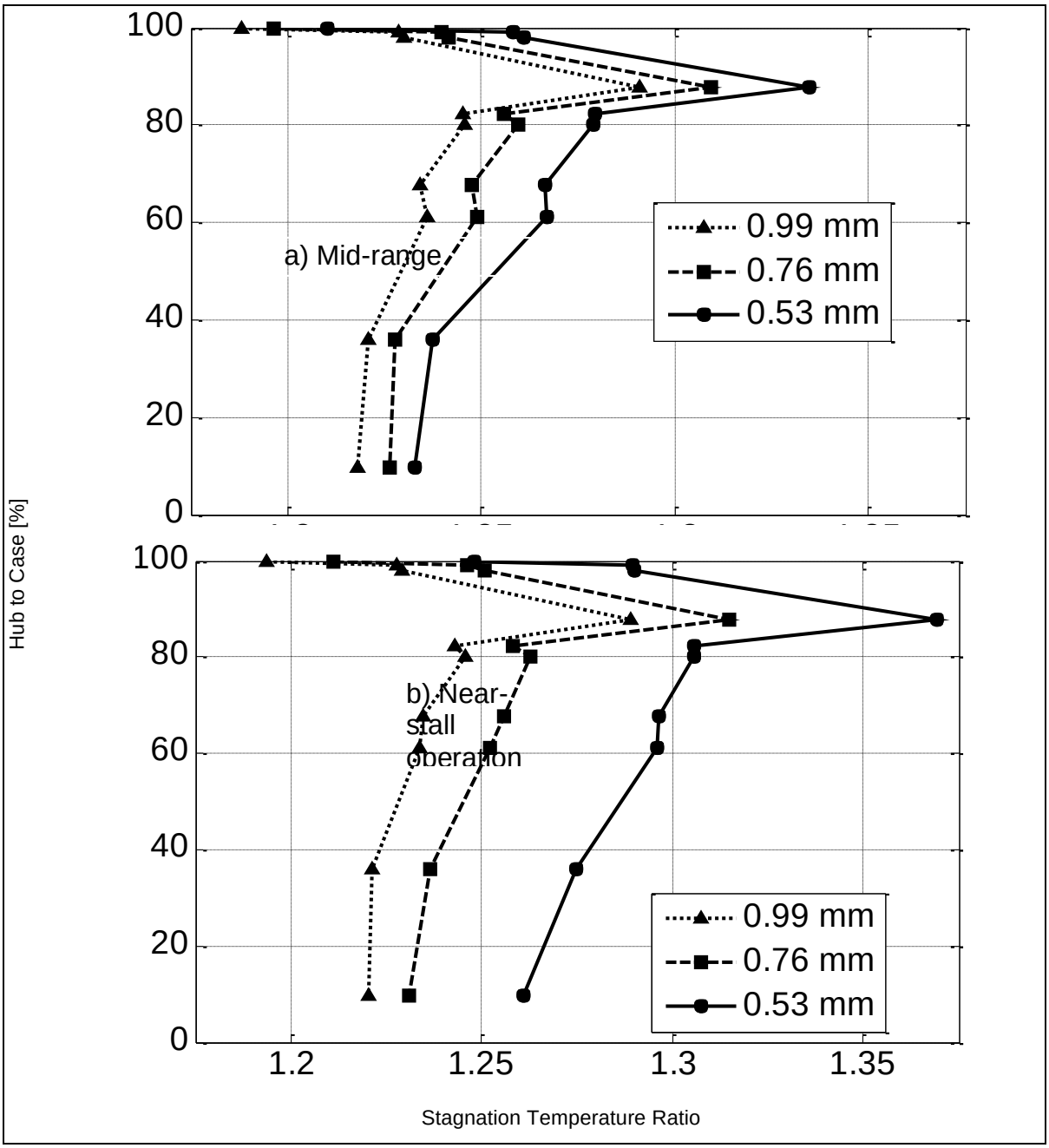

Fig. 41, 100% speed stagnation temperature ratio profiles.

CONCLUSIONS

The goal of this study was to design, test, and evaluate a transonic axial compressor rotor with splitter blades and all objectives were met. In accomplishing these objectives, several outcomes have been achieved:

1. A new design procedure has been developed and documented that uses commercial-off-the-shelf software for the geometric rendering and analysis of a transonic compressor rotor.
2. MATLAB was used to script the whole design procedure by performing a preliminary tip section design, defining blade parameters, and controlling both SolidWorks and ANSYS-CFX.
3. During a design cycle a complete constant speedline of the compressor was analyzed from open throttle (choke) to stall conditions. This allowed overall performance to be evaluated and compared during each cycle.
4. After restacking of the blade profiles and including fillet radii at the blade roots the design was frozen. A solid blisk (blade and disk) was machined out of 7075-T6 aluminum alloy and tested in the Transonic Compressor Rig.
5. This study advanced the understanding of splitter blade geometry, placement, and performance benefits. In particular, it was determined that moving the splitter blade forward in the passage between the main blades, which was a departure from the trends demonstrated in the few available previous transonic axial compressor splitter blade studies, increased the mass flow range with no loss in overall performance.
6. With a large 0.91 mm (0.036 in) tip clearance, to preserve the integrity of the rotor, the experimentally measured peak total-to-total pressure ratio was 1.69 and the peak total-to-total isentropic efficiency was 72 percent at 100 percent design speed. Additionally, a higher than predicted 7.5 percent mass flow rate range was experimentally measured, which would make for easier engine control if this concept were to be included in an actual gas turbine engine.

The first completed experimental test of a splittered transonic compressor rotor as part of a program to test novel geometries has been completed. In the experiments presented here, three different tip gaps were tested and three sets of data obtained. The test were completed over a wide speed range and this coupled with the varying tip gaps means that the data is applicable to transonic front stages with small tip gap to blade height ratios and also to subsonic core stages with larger tip gap to blade height ratios. Non-dimensionalized effects of the increase of the tip gap on the efficiency are presented.

The data presents a useable test case as the inlet conditions are well documented. These include the gas mixture properties taking into account water vapor, which has a small but measureable effect. Also given are the absolute pressure and temperature at the inlet to the compressor, which are important in simulating the correct Reynolds numbers. The geometry is available upon request.

REFERENCES

1. Wennerstrom, A. and Hearsey, R., 1971, “The Design of an Axial Compressor Stage for a Total Pressure Ratio of 3 to 1,” Aerospace Research Laboratories report AR 71-0061, Wright-Patterson AFB, Dayton, Ohio
2. Wennerstrom, A. and Frost, G., 1974, “Design of a Rotor Incorporating Splitter Vanes for a High Pressure Ratio Supersonic Axial Compressor Stage,” Aerospace Research Laboratories report AR 74-0110, Wright-Patterson AFB, Dayton, Ohio
3. Wennerstrom, A., Buzzel, W. and Frost, G., 1975, “Test of a Supersonic Axial Compressor Stage Incorporating Splitter Vanes in the Rotor,” Aerospace Research Laboratories report AR 75-0165, Wright-Patterson AFB, Dayton, Ohio
4. Tzuoo, K., Hingorani, S. and Sehra, A., 1990, “Design Methodology for Splittered Axial Compressor Rotors,” ASME Paper 90-GT-66.
5. McGlumphy, J., Ng. W-F., Wellborn, S. and Kempf, S., 2010, “3D Numerical Investigation of Tandem Airfoils for a Core Compressor Rotor,” ASME *Journal of Turbomachinery*, Vol. 132.
6. Smith, L. H., 1993, “Wake Ingestion Propulsion Benefit,” AIAA *Journal of Propulsion and Power*, 9(1):74-82.
7. Vo, H.D., 2001, “Role of Tip Clearance Flow on Axial Compressor Stability,” PhD thesis, Mass. Inst. Technolgy, Cambridge, MA.
8. Tan, C. S., Day, I., Morris, S. and Wadia, A., “Spike-Type Compressor Stall Inception, Detection and Control,” 2010, Ann. Rev. Fluid Mech. 42: pp 275-300.
9. Bhargava, R.K. & Gopalakrishnan, G., 1978, “Optimising Splitter Vane Locations Using the Method of Singularities,” Proc. of the First International Conference on Centrifugal Compressor Technology, Madras, India.
10. Ogawa, T. & Gopalakrishnan, G., 1977, “Flow Calculation in a Centrifugal Impeller by the Method of Singularities and its Experimental Verification,” Proc. of the Seventh National Conference on Fluid Power and Fluid Mechanics, Baroda, India
11. Ogawa, T. & Gopalakrishnan, G., 1981, “Use of Splitter Vanes in Centrifugal Compressor Impellers,” Proc. of the Eighth Canadian Congress of Applied Mechanics, Moncton, Canada
12. Fabri, J., 1978, “Flow Distribution in a Radial Impeller with Splitter Vanes,” Proc. of the First International Conference on Centrifugal Compressor Technology, Madras, India
13. Millour, V., 1988, “3D Flow Computations in a Centrifugal Compressor with Splitter Blade Including Viscous Effect Simulation,” 16th Congress, International Council of Aeronautical Societies, Volume 1, pp. 842 – 847
14. McGlumphy, J., 2008, “Numerical Investigation of Subsonic Axial-Flow Tandem Airfoils for a Core Compressor Rotor,” PhD Dissertation, Virginia Polytechnic Institute and State University
15. Sanger, N. L, 1996, "Design of a Low Aspect Ratio Transonic Compressor Stage Using CFD Techniques," ASME *Journal of Turbomachinery,* Vol. 118, pp. 479 - 491.
16. Sanger, N. L., 1999, “Design Methodology For The NPS Transonic Compressor,” Turbopropulsion Laboratory, Naval Postgraduate School, Tech Note 99-01.
17. Drayton, S., “Design, Test and Evaluation of a Transonic Axial Compressor Rotor with Splitter Blades,” PhD Dissertation, Dept of Mechanical and Aerospace Engineering, Naval Postgraduate School, Monterey CA, 2013.
18. Grossman, B. L., “Testing And Analysis Of A Transonic Axial Compressor,” M.S. Thesis, Dept. Aeronautical and Astronautical Eng, Naval Postgraduate School, Monterey CA, 1997.

19. Londono, A., “Near-stall modal disturbances within a transonic compressor rotor,” M.S. thesis, Dept. Mechanical and Aerospace Eng, Naval Postgraduate School, Monterey CA, 2011.
20. Payne, T. A., “Inlet Flow-Field Measurements Of A Transonic Compressor Rotor Prior To And During Steam-Induced Rotating Stall,” M.S. thesis, Dept. Mechanical and Aerospace Eng, Naval Postgraduate School, Monterey CA, 2005.
21. Wisler, D.C., "Advanced Compressor and Fan Systems," lecture notes, General Electric Aircraft Engine Business Group, Cincinnati, OH.